Ofioliti, 2026, 51 (2), 187-206 - doi: 4454/ofioliti.v51i2.587

SPATIAL VARIATION IN SAMAIL METAMORPHIC SOLE PROTOLITHS: A REGIONAL-SCALE ISOTOPIC (HF, ND, U-PB) AND TRACE-ELEMENT PERSPECTIVE

Joshua M. Garber*,,✉, Matthew Rioux***,°, Michael P. Searle°°, Peter L. Baker°°°, Jeffrey Vervoort°°°, Alexander Nikitin**, Andrew J. Smye**, Tyler Ambrose• and Isabel Fendley****

* *School of Earth and Environmental Sciences, University of St Andrews, UK.*
** *Department of Geosciences, The Pennsylvania State University, USA.*
*** *Department of Earth Science, University of California Santa Barbara, USA.*
° *Earth Research Institute, University of California Santa Barbara, USA.*
°° *Oxford University, UK.*
°°° *Washington State University, USA.*
• *Yukon Geological Survey, Canada.*
✉ *Corresponding author, e-mail: jg340@st-andrews.ac.uk*

Keywords: Ophiolite; Metamorphic sole; Samail; Sm-Nd isotopes; Lu-Hf isotopes; Trace elements; Zircon; U-Pb dating.

ABSTRACT

Metamorphic soles beneath ophiolites contain important records of subduction initiation; protoliths of these sole rocks preserve information about tectonic processes occurring prior to and during ophiolite emplacement. The Samail Ophiolite – the largest and best exposed ophiolite on Earth – exposes metamorphic soles at its base spanning hundreds of kilometers along its length, but there are a limited number of sole geochemical data from few outcrops. Here, we present a trace-element, isotopic (Hf and Nd), and geochronological (zircon U-Pb) dataset spanning the entire length of the ophiolite, which we use to interpret the tectonic setting and thermal mechanisms driving ophiolite formation and thrusting. To constrain the earliest perspective on ophiolite emplacement, we obtained whole-rock geochemical information from n=36 garnet- and clinopyroxene-bearing sole amphibolites at the top of each sole section. Most of these high-grade sole rocks have affinities toward enriched mid-ocean ridge basalt (E-MORB) compositions, nominally matching earlier inferences for derivation of the metamorphic sole from the Haybi Complex that immediately underlies the sole. This interpretation is also supported by detrital zircons from one mixed sole amphibolite-metasediment that yield a Carboniferous maximum depositional age, as well as a compiled sole-Haybi Carboniferous Sm-Nd whole-rock isochron. However, a subset of the sole amphibolites from south Oman and the UAE exhibit N-MORB-like elemental and isotopic characteristics. This observation suggests either that there is an unidentified N-MORB-like member of the Haybi Complex; that there is another, unidentified Indian Ocean MORB source for the Samail sole; or that the V1 volcanics (Geotimes unit) of the ophiolite may have supplied some of the rocks now forming the metamorphic sole. The first two of these would suggest ≥150 Ma protolith ages at the time of subduction initiation, while the latter of these would indicate mixing between protoliths of variable ages, despite the absence of variations in peak sole P-T along the ophiolite. Regardless of protolith age, the data presented in this study reveal multiple scales of heterogeneity for the basaltic protolith of rocks composing the uppermost Samail sole.

INTRODUCTION

Ophiolites represent a window into two major geologic processes: the formation of oceanic crust at mid-ocean ridges, and the consumption of oceanic crust during subduction. Metamorphic soles welded to the base of ophiolites present a key opportunity to understand the latter of these processes, as amphibolites within soles are thought to reflect the first pieces of oceanic crust subducted beneath a given ophiolite (e.g., Agard et al., 2016), providing a key window into the structural development and thermal architecture leading up to and during the initial stages of ophiolite formation. Since initial efforts in the 1970s-1980s (e.g., Williams and Smyth, 1973; Malpas, 1979; Searle and Malpas, 1980; Ghent and Stout, 1981; Jamieson, 1986), much of the focus on metamorphic soles has revolved around their remarkably similar mineralogy and P-T conditions globally beneath different ophiolites, which suggests consistency in the geodynamic mechanisms that form soles spatially within any single ophiolite and among ophiolites throughout Earth history (Wakabayashi and Dilek, 2000, 2003; Agard et al., 2016).

While ophiolite geochemistry has frequently been used to understand the tectonic configurations fostering ophiolite formation (e.g., Miyashiro, 1973; Alabaster et al., 1982; Pearce et al., 1984; Dilek and Furnes, 2014), the geochemistry of metamorphic soles has less often been used for the same purpose (Searle and Malpas, 1982; Savci, 1988; Carosi et al., 1996; Parkinson, 1998; Dimo-Lahitte et al., 2001; Searle and Cox, 2002; Gaggero et al., 2009; Guilmette et al., 2009; Farahat, 2011; Cluzel et al., 2012; Keenan et al., 2016; Šegvić et al., 2018; Ullah et al., 2021; Xin et al., 2021; Valera et al., 2022a; Fournier-Roy et al., 2023; Mackay-Champion et al., 2024). These and other studies have observed differences in geochemistry from the top to the bottom of the sole section (Ishikawa et al., 2005; Dewey and Casey, 2013; Xin et al., 2021) or for several mixed protoliths (Carosi et al., 1996; Gaggero et al., 2009), and many soles contain evidence for metasomatic overprinting (Ishikawa et al., 2005; Valera et al., 2022a, b) that also extends to the overlying mantle section (Yoshikawa et al., 2015; Ambrose et al., 2018; Prigent et al., 2018). However, given the spatially limited exposures of most soles relative to their overlying ophiolites, many of these studies are on small and/or dismembered outcrops that lack accompanying high-resolution geochronological or other data.

The Samail Ophiolite of Oman and the United Arab Emirates – the world's largest and best exposed ophiolite – presents a unique opportunity to understand the tectonic context of ophiolite formation using the geochemistry of the metamorphic sole. Such an opportunity is supported by numerous studies of ophiolite geochronology and geochemistry (Pearce et al., 1981; Tilton et al., 1981; Alabaster et al., 1982; Ishikawa et al., 2002; Godard et al., 2003; Godard et al., 2006; Kusano et al., 2012; Rioux et al., 2013; Belgrano and Diamond, 2019; Belgrano et al., 2019; Rioux et al., 2021a; Rioux et al., 2021b) and numerous studies on sole geochronology and geochemistry (Searle and Malpas, 1980; Tilton et al., 1981; Searle and Malpas, 1982; Ziegler et al., 1991b; Hacker et al., 1996; Ishikawa et al., 2005; Warren et al., 2005; Rioux et al., 2016; Roberts et al., 2016; Soret et al., 2017; Guilmette et al., 2018; Garber et al., 2020; Kim et al., 2020; Soret et al., 2022; Rioux et al., 2023; Garber et al., 2025). There are also exposures of the metamorphic sole spanning nearly the entire length of the ophiolite, although the highest-grade soles are more spatially restricted (e.g., Rioux et al., 2023). However, despite the significant number of previous studies identifying and describing the supra-subduction zone evolution of the Samail Ophiolite (Pearce et al., 1981; Alabaster et al., 1982; Ishikawa et al., 2002; Goodenough et al., 2010; Kusano et al., 2012; MacLeod et al., 2013; Belgrano and Diamond, 2019; Rioux et al., 2021b), only a few studies have investigated the geochemistry of the metamorphic sole to understand its protolith (Searle and Malpas, 1982; Ishikawa et al., 2005; Kim et al., 2020), which has direct bearing on the nature of the lower plate during ophiolite obduction.

Here, we present a new geochemical dataset from 36 high-grade garnet-clinopyroxene amphibolites from sole exposures spanning the length of the entire Samail Ophiolite. These samples were collected from the top of each sole outcrop, representing samples of the earliest material thrust beneath the ophiolite at each location. The dataset includes whole-rock trace-element and isotopic (Nd, Hf) data, as well as detrital zircon U-Pb and trace-element data from one sample of partial metasedimentary origin. We compare these data to two proposed protoliths for the metamorphic sole: the Haybi Complex thrust sheet beneath the sole, which includes Permian-Triassic limestones and varied basalts, as well as likely Jurassic-Cretaceous deep-sea cherts and alkali basalt intrusions (Searle et al., 1980; Searle and Malpas, 1980, 1982; Searle, 1984, 2007) and the earliest volcanic section (V1) of the Cenomanian Samail Ophiolite itself (e.g., Godard et al., 2003; Godard et al., 2006). With these comparisons, we conclude by discussing the tectonic setting of ophiolite formation and the earliest phase of ophiolite obduction.

GEOLOGICAL BACKGROUND

The Samail Ophiolite (Fig. 1) contains an archetypal cross-section through fast-spreading oceanic lithosphere, including significant portions of crust and upper mantle (Glennie et al., 1973; Hopson et al., 1981; Pallister and Hopson, 1981; Lippard et al., 1986). The architecture of the ophiolite includes from top to bottom: pillow basalts; sheeted dikes; discontinuous tonalitic intrusives (plagiogranites, which also occur elsewhere in the crustal section); isotropic, flow-foliated, and cumulate gabbros; a Moho transition zone with dunites, wehrlites, pyroxenites, harzburgites, gabbros, and podiform chromitites; and depleted harzburgite (e.g., Nicolas et al., 2000). The earliest, most volumetrically dominant "V1" lavas and intrusives are generally similar to other Indian Ocean mid-ocean ridge basalts (MORB) (e.g., Godard et al., 2006), although major- and trace-element data indicate that they formed in the presence of some H_2O in their source and likely crystallized after subduction had already initiated (e.g., MacLeod et al., 2013). The V1 rocks (also termed the "Geotimes" unit) were succeeded by a second "V2" magmatic suite ("Lasail" unit), including but not limited to wehrlites and boninites, that reflect remelting of a depleted mantle lithosphere in the presence of higher H_2O and large-ion lithophile elements (e.g., Godard et al., 2003; Koepke et al., 2009; Kusano et al., 2012; Haase et al., 2016; Belgrano and Diamond, 2019), consistent with forearc magmatism above an active subduction zone. Finally, there are a suite of felsic dikes and sills that crosscut the mantle section of the ophiolite; the composition of these intrusions reflects mixed metasediment-amphibolite melts with or without a mantle component (Haase et al., 2015; Rollinson, 2015; Spencer et al., 2017; Rioux et al., 2021a). These three magmatic suites crystallized in sequence, with V1 zircon U-Pb crystallization dates ranging from 96.2–95.6 Ma and V2 from 95.6–95.2 Ma; in Oman the felsic mantle dikes crystallized over a narrow time interval from 95.2–95.0 Ma, whereas in the UAE these dike dates extend to 91.0 Ma (Rioux et al., 2013; Rioux et al., 2021b). The magmatic compositional sequence and timing preserved in the ophiolite is similar to that of the Izu-Bonin-Mariana forearc, consistent with the formation of the ophiolite during subduction initiation (Ishizuka et al., 2011; Belgrano and Diamond, 2019; Rioux et al., 2021b).

Metamorphic soles occur intermittently along the base of ophiolitic harzburgites along nearly the entire length of the Samail Ophiolite, with exposed thicknesses ranging from a few meters up to 500 m. Although there are consistent characteristics throughout many of these outcrops, there is significant heterogeneity among them and there are also significant geographic changes in these exposures. The most classic, well-studied metamorphic sole exposures exhibit a temperature gradient with increasing structural depth from the sharply-defined Samail thrust with the overlying ophiolite (Searle et al., 2022). Lithologically, these sections grade from upper amphibolite to granulite facies, dominantly mafic, garnet-clinopyroxene amphibolites (1.0–1.5 GPa, 750–900 ºC), to amphibolite and greenschist facies, mixed metabasalts and metasediments that are underlain by unmetamorphosed rocks (Ghent and Stout, 1981; Gnos, 1992; Hacker and Mosenfelder, 1996; Hacker and Gnos, 1997; Gnos, 1998; Searle and Cox, 2002; Cowan et al., 2014; Soret et al., 2017; Garber et al., 2020; Ambrose et al., 2021; Kotowski et al., 2021). Whereas coarse-grained metagabbros have been reported from other metamorphic soles (e.g., Fournier-Roy et al., 2023), none have been reported from Samail. Discrete slices with distinct protoliths are apparent throughout all sole exposures (Ishikawa et al., 2005; Soret et al., 2017), but the downward continuity and evolution of the thermal gradient throughout the sole metamorphic history is unclear (Garber et al., 2020), and each set of higher-T rocks has undergone retrogression and overprinting by successively lower-temperature conditions (Soret et al., 2019; Ambrose et al., 2021). Some studies have demonstrated a pressure gradient with structural depth (Gnos, 1998; Garber et al., 2020), while others have shown that the cooler rocks at the base of metamorphic soles could have been metamorphosed under similar pressures to those at the top (Ambrose et al., 2021; Kotowski et al., 2021). In many outcrops, the top, highest-grade, garnet-bearing rocks have either been excised or were never present. Where present, however, the thickness of the garnet-bearing soles changes from the south to the north, from ≤5 m in the Wadi Tayin massif, to ≤50 m in the Sumeini Window, to ≤85 m in the Asimah Window (Hacker and Mosenfelder, 1996; Soret

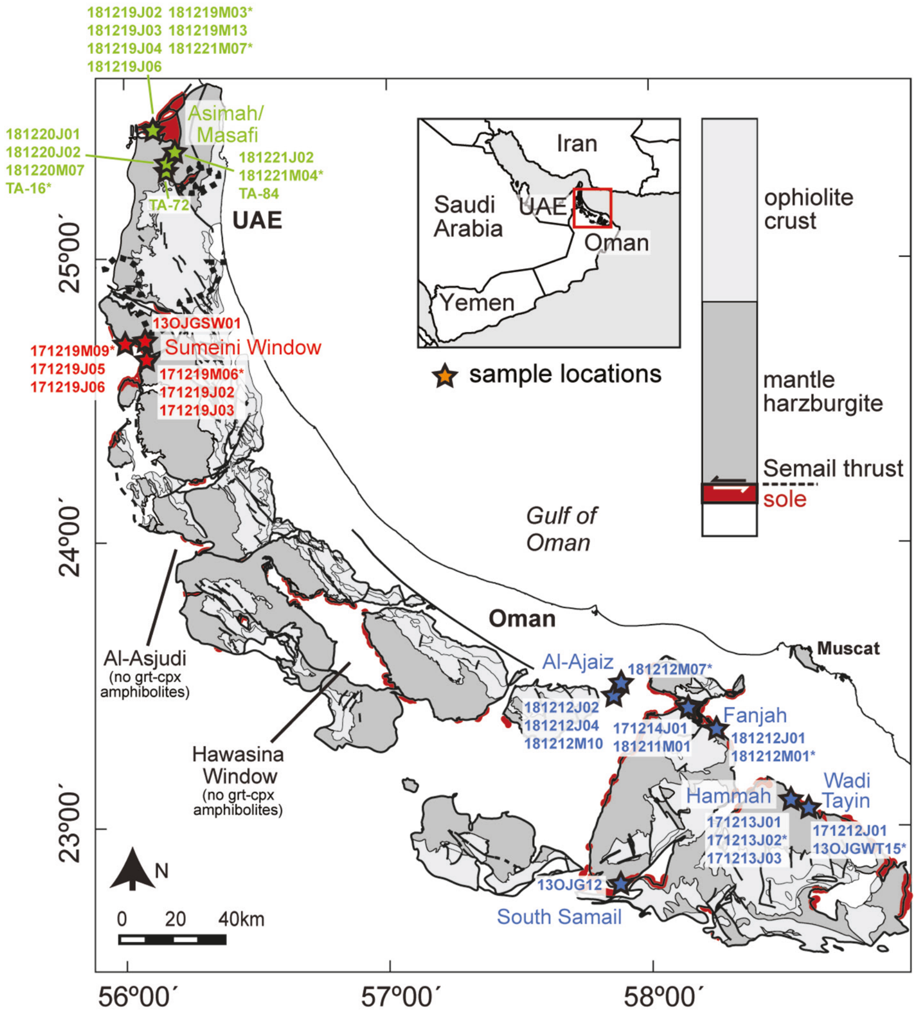

Fig. 1 - Tectonic map of the Samail Ophiolite subdivided into crust, mantle, and metamorphic sole. Sample locations from this study are identified by stars coloured by three regional clusters of data. Trace-element data are presented for all the samples noted in the Fig.; sample names with an asterisk are those for which new isotopic data (Nd, Hf) are presented.

et al., 2017; Ambrose et al., 2021). Some of these thickness variations can be explained by imbricated fault repetitions (Searle and Malpas, 1980; Cowan et al., 2014).

A diversity of metamorphic ages has been reported for the Samail metamorphic sole. While an exhaustive discussion of these ages is beyond the scope of this paper (see Searle et al., 2025), reported Samail sole ages can broadly be classified into two contrasting interpretive frameworks. The first relies on high-precision zircon U-Pb TIMS data coupled to zircon LA-ICPMS trace element measurements (Rioux et al., 2016; Rioux et al., 2023) as well as garnet diffusion modelling (Garber et al., 2025), which shows that the highest-grade rocks in the metamorphic sole underwent prograde to peak conditions no more than ~500 kyr prior to ophiolite formation, with upper amphibolite to granulite-facies zircon growth (bracketing garnet growth) occurring from 96.7–95.2 Ma. Lower-grade, structurally lower, garnet-free amphibolites – as well as leucosomes that crosscut the higher-grade garnet-clinopyroxene amphibolites – yield younger zircon ages at each outcrop, with dates from 96.2–94.7 Ma (Rioux et al., 2016; Rioux et al., 2023). An amphibolite-facies garnet-bearing metasediment within the uppermost unit at Wadi Tayin also yielded a Lu-Hf garnet-whole rock isochron date of 93.0±0.5 Ma for garnet growth (Garber et al., 2020). There is also a spatial progression of high-grade metamorphic zircon ages, with the oldest U-Pb dates occurring at the Sumeini Window in northern Oman, the youngest occurring in Wadi Tayin in southern Oman, and dates spanning this entire range occurring in the Masafi Window in the UAE (Rioux et al., 2023). Notably, such a progression is also subtly present in hornblende and white mica $^{40}Ar/^{39}Ar$ cooling dates, which suggest rapid cooling of the high-temperature portion of the sole from 95 to 93 Ma (Hacker et al., 1996).

A second set of geochronology, including ~104-103 Ma garnet Lu-Hf dates (Guilmette et al., 2018) as well as ~100 Ma titanite and monazite LA-ICPMS U-Pb and trace-element data (Soret et al., 2022), suggests that metamorphism may have preceded the crystallization of the Samail Ophiolite by 8–10 Myr, which has been interpreted as the timing of forced subduction initiation. In this context, the zircon U-Pb dates from 96.7 Ma onwards were interpreted to represent a purely cooling related signal, during the crystallization of post-peak melts (Guilmette et al., 2018). Recently, however, several issues have been identified with each of these datasets. For example, the garnet Lu-Hf dates have spurious lower $^{176}Hf/^{177}Hf$ intercepts that clearly deviate from those determined by other methods in Samail amphibolites (discussed in further detail with data from this study, below). Additionally, an attempt to reproduce the Guilmette et al. (2018) Lu-Hf date yielded a significantly younger, internally consistent, garnet-whole rock-zircon Lu-Hf date from one of the same outcrops dated in that study (97.9±0.5 Ma: Garber et al., 2025). The ~100 Ma titanite and monazite U-Pb ages also rely on choices made during data reduction, while the underlying data do not require ~100 Ma (or older) metamorphism and are equally consistent with the younger, higher-precision zircon TIMS dates. Considering these factors, we rely on the

96.7–95.2 Ma high-precision zircon dates from Rioux et al. (2023) as representative of the timing of prograde to peak metamorphism in the high-grade garnet-clinopyroxene amphibolites analysed in this study.

Several possible protoliths for the Samail metamorphic sole have been identified. Underlying the sole is a series of stacked, unmetamorphosed thrust sheets reflecting the architecture of the former passive margin, from distal Haybi volcanics, sediments, and "exotic" limestone seamounts, to more proximal Hawasina siliciclastics, cherts, and carbonates, to Sumeini Group shelf edge and slope sediments that overthrust autochthonous Arabian plate rocks (Glennie et al., 1973; Searle et al., 1980; Searle and Malpas, 1980, 1982). The structurally highest, Haybi thrust sheet immediately beneath the sole contains a significant thickness of basaltic rocks, with E-MORB-like, incompatible-element depleted to "transitional" (i.e., slightly more enriched) tholeiites interspersed with limestones toward the top and alkaline, within-plate volcanics at their base (Searle et al., 1980; Searle and Malpas, 1980, 1982; Searle, 2007). Some exposures of the Haybi Complex in the Dibba Zone (UAE) also contain significant fractions of carbonatite lavas (Ziegler et al., 1991a; Ziegler et al., 1991b). K-Ar ages from biotite separates in three different Haybi exposures yielded cooling ages of 233±9, 219±9, and 200±8 Ma, suggesting their derivation during Triassic rifting (Searle et al., 1980). By comparing the geochemistry of Haybi volcanics with the geochemistry of sole amphibolites, it has been previously suggested that the upper Haybi tholeiite member is a viable protolith for both high- and low-grade metamafic sole rocks (Searle and Malpas, 1980; Searle and Cox, 2002), although this correlation was in some cases recognized as tenuous (Searle and Malpas, 1982). This observation also comports with the frequent occurrence of intercalated amphibolites and metacarbonates in several classic sole outcrops (e.g., Searle and Graham, 1982). On the other hand, Ishikawa et al. (2005) performed a major- and trace-element transect through the Wadi Tayin exposure of the metamorphic sole in Oman, and found at least three different metabasaltic protoliths represented at a single outcrop. These included E-MORB characteristics preserved in the topmost, highest-grade clinopyroxene-bearing amphibolites; compositional similarities to Samail V1 and other Indian Ocean N-MORB preserved in garnet- and clinopyroxene-free amphibolites; and a unique, light rare-earth-element (LREE) and high-field strength element depleted but large-ion lithophile-rich island arc tholeiite contained within a folded chert layer, that they ascribed to probable Samail V2 origin. Finally, TIMS and LA-ICPMS U-Pb dating and trace-element analyses of detrital zircon from cherts within the metamorphic sole section showed evidence that some sole protoliths were affected by sedimentation (either wind-blown or subaqueous) until at least 107 Ma (Garber et al., 2020). While some authors have suggested that these young ages may represent metamorphic zircon ages (Soret et al., 2022; Ring et al., 2024), recent detrital zircon analysis of the Cretaceous Muti Formation elsewhere in Oman – which is associated with ophiolite emplacement – show similarly aged detrital zircons (100-120 Ma; Ahmed Abbasi et al., 2026).

SAMPLE DESCRIPTIONS

We collected samples of the structurally highest metamorphic sole amphibolites spanning the entire length of the Samail Ophiolite (Fig. 1, Table 1). These include rocks taken from multiple locations within classic, well-studied outcrops (e.g., Wadi Tayin, Sumeini Window, Asimah), as well as outcrops described in the literature but without any previous published data (e.g., Fanjah, Al-Ajaiz). These outcrops are generally clustered in three geographic regions – south Oman, Sumeini Window, and Asimah/Masafi (UAE) – which is how the data are presented below. Each of these outcrops exhibits high-grade garnet-clinopyroxene amphibolites at

Table 1 - Sole Amphibolite samples

Sample	Location	Longitude	Latitude
13OJG12	South Samail	57.8897	22.8121
171212J01	Wadi Tayin	58.5972	23.0558
13OJGWT15*	Wadi Tayin	58.6021	23.0621
171213J01	Hammah	58.5448	23.0984
171213J02*	Hammah	58.5358	23.1006
171213J03	Hammah	58.5420	23.1017
181212J01	Fanjah	58.2412	23.3422
181212M01*	Fanjah	58.2414	23.3428
181211M01	Fanjah	58.1482	23.4302
171214J01	Fanjah	58.1482	23.4302
181212J02	Al Ajaiz	57.8743	23.4736
181212J04	Al Ajaiz	57.8743	23.4736
181212M10	Al Ajaiz	57.8742	23.4736
181212M07*	Al Ajaiz	57.8963	23.5090
171219M06*	Sumeini E	56.0739	24.6468
171219J02	Sumeini E	56.0739	24.6468
171219J03	Sumeini E	56.0739	24.6468
171219M09*	Sumeini W	56.0074	24.6967
171219J05	Sumeini W	56.0074	24.6967
171219J06	Sumeini W	56.0074	24.6967
13OJGSW01	Sumeini N	56.0750	24.6988
TA-72	Masafi S	56.1572	25.3114
181220M07	Masafi S	56.1571	25.3235
181220J02	Masafi S	56.1571	25.3235
TA-16*	Masafi S	56.1566	25.3244
181220J01	Masafi S	56.1568	25.3246
181221M04*	Masafi E	56.1801	25.3584
181221J02	Masafi E	56.1801	25.3584
TA-84	Masafi E	56.1790	25.3590
181221M07*	Masafi NW	56.1072	25.4438
181219J04	Masafi NW	56.0958	25.4459
181219J03	Masafi NW	56.0956	25.4464
181219J06	Masafi NW	56.0936	25.4464
181219J02	Masafi NW	56.0958	25.4465
181219M13	Masafi NW	56.0935	25.4466
181219M03*	Masafi NW	56.0963	25.4466

*analysed for Nd and Hf isotopes.

their top, other than a single outcrop from South Samail where garnet was not observed. However, the South Samail sample is highly sheared, contains clinopyroxene, and exhibits zircon geochemical characteristics consistent with the former presence of garnet interpreted to have been resorbed upon retrogression (Rioux et al., 2023).

All remaining samples exhibit the same peak, granulite-facies assemblage of garnet, clinopyroxene, brown hornblende, plagioclase, ilmenite, and apatite, occurring as discrete mm- to cm-scale anhedral clots; these peak-assemblage phases are set in a matrix of retrogressed brown to green amphibole and plagioclase (Fig. 2). Peak pressure-temperature conditions for these granulite-facies rocks have been reported from several of the outcrops sampled in this study, including Wadi Tayin (≥1.0 GPa, ~820ºC: Hacker and Mosenfelder, 1996; Cowan et al., 2014; Soret et al., 2017), Sumeini Window (~1.0 GPa, ~850ºC: Cowan et al., 2014; Soret et al., 2017), Asimah Window/Masafi South (1.0-1.2 GPa, 700-900ºC: Gnos, 1998; Ambrose et al., 2021), and Wadi Khubakhib/Masafi Northwest (~1.0 GPa, ~850ºC: Soret et al., 2017). In a few samples mostly from southern Oman, rutile grains occur either as oriented needles or equant grains within garnet cores, but the remaining samples exhibit ilmenite associated with the peak granulite-facies assemblage (particularly in garnet rims), and titanite associated with the prograde (as garnet core inclusions) or retrograde assemblage (in the matrix). In some samples, the cores of large garnet porphyroblasts contain relics of prograde phases, including prograde green hornblende, titanite, and plagioclase (Fig. 2a-c, e), although the majority of garnets in each sample lack these cores (Fig. 2d, f) (Garber et al., 2025). Garnet grains in some samples are pervasively chloritized, and most plagioclase grains have likewise been sericitized, although fresh plagioclase is present in about a third of samples. Late carbonate-quartz veins crosscut several samples and were avoided during geochemical sampling. Despite all rocks containing a near-identical peak assemblage, there are differences in texture, fabric intensity, grain size (particularly in garnet), and extent of retrogression; these will be discussed elsewhere (Garber et al., in prep), although we did not identify any obvious correlation between these textural variations and the whole-rock geochemistry of each sample, discussed below.

ANALYTICAL TECHNIQUES

Rock chips free of weathering-related alteration and carbonate veining were isolated from each hand sample for analysis. All trace-element data from this study are presented in Table S1. Whole rock major and trace elements were first determined by X-ray fluorescence at Franklin and Marshall College, following the methods of Mertzman (2000) and Waterton et al. (2020), with ferrous/ferric iron determined by titration (Reichen and Fahey, 1962). Because the whole-rock major element chemistry of the sole amphibolites is often affected by processes superimposed on the inherited protolith composition, including metasomatism during peak metamorphism (e.g., Ishikawa et al., 2005; Valera et al., 2022a), we do not include these data in Table S1 nor discuss them here, as these will be addressed in a subsequent contribution. Sample chips were crushed in alumina equipment and powdered using a Spex ceramic-lined mixer mill, until all powder passed through a clean 80-mesh sieve. After determination of loss-on-ignition (LOI), which creates an anhydrous powder, trace-element analysis was performed on a pressed briquette composed of sample powder (7 g) mixed with high-purity copolywax powder (1.4 g). Data are reported for Ti, Rb, Sr, Y, Zr, V, Ni, Cr, Nb, Ga, Cu, Zn, Co, Ba, U, Th, La, Ce, Sc, Pb, and Mo. The data for unknowns were calibrated against rock standards prepared in the same fashion, with 50-60 points per calibration curve.

The samples were subjected to additional trace-element analysis for rare-earth elements (REE), Hf, Ta, U, and Th by Actlabs (Ontario, Canada) using the “4B2-std” protocol. The samples were fluxed and fused with lithium metaborate and lithium tetraborate in an induction furnace, which was dissolved into a 5% nitric acid solution with an internal standard. Trace elements were measured using a Perkins Elmer Elan 9000 inductively coupled plasma mass spectrometer (ICPMS). Detections limits for all elements were 0.05-0.1 ppm, except for Hf (0.2 ppm). Accuracy was assessed using a range of standards that underwent the same analytical routine, and data for all elements in these standards were within ≤5% of their reported values. Likewise, analytical precision was assessed using duplicates of the same rock standards as well as our samples, and consistently found to be ≤5% RSD.

Mercury concentration measurements were measured on sample powders using a Lumex RA-915M direct mercury analyser with Pyro 915+ attachment at The Pennsylvania State University. Samples and standards were weighed out in quartz boats and heated to 900ºC to liberate Hg for analysis by atomic absorption spectroscopy (see also Roy and Bose, 2008; Marie et al., 2015). The instrument was first calibrated using NIST SRM 2587 (Hg = 290 ± 9 ppb) of varying masses. Throughout the measurement session, we ran aliquots of USGS BIR-1 basalt powder as a precision monitor, yielding an average of 9.2 ± 0.6 ppb (2 s.d.; n = 8). Approximately 200-400 mg of powder was weighed out per sample, and each sample was measured in duplicate; reported results are averages of the two measurements, which were typically within 20% of each other.

Statistical analyses on the trace-element data were performed in MATLAB®. A residual that sums each analysis to 100 wt % (1,000,000 ppm) was added prior to log-normalizing the data using a centered log-ratio transformation (Aitchison, 1982), which were then centred (mean = 0) and scaled (standard deviation = 1). Principal components analysis was applied using the pca function. The significance of each principal component (PC) is discussed below in terms of the per cent variance of the dataset that it explains; that is, the ratio of each PC eigenvalue normalized to the sum of all eigenvalues.

Neodymium and hafnium isotopes were measured on a subset of samples at the Radiogenic Isotope and Geochronology Laboratory at Washington State University. Each sample consisted of a ~250 mg aliquot of whole rock powder; samples were digested, spiked, and underwent ion-exchange chromatography, prior to measurement using a Neptune Plus MC-ICPMS, following the methods outlined in Johnson et al. (2018). ε_{Hf} and ε_{Nd} were calculated using the chondritic uniform reservoir (CHUR) parameters from Bouvier et al. (2008) ($^{176}Hf/^{177}Hf_{CHUR}$ = 0.282785 ± 0.000011, $^{176}Lu/^{177}Hf_{CHUR}$ = 0.0336 ± 0.0001; $^{143}Nd/^{144}Nd_{CHUR}$ = 0.512630 ± 0.000011, $^{147}Sm/^{144}Nd_{CHUR}$ = 0.1960 ± 0.0004); errors on ε_{Hf} and ε_{Nd} were propagated for sample isotopic ratios and age only (assumed to be 96 ± 1 Ma). To test for the influence of potentially inherited phases not in isotopic equilibrium with the whole rock aliquot, we subjected two samples (171213J02, Hammah; 181219M03, Asimah) to both tabletop (on a hotplate only) and pressure-assisted digestion (in a Parr bomb); these duplicates yielded data within

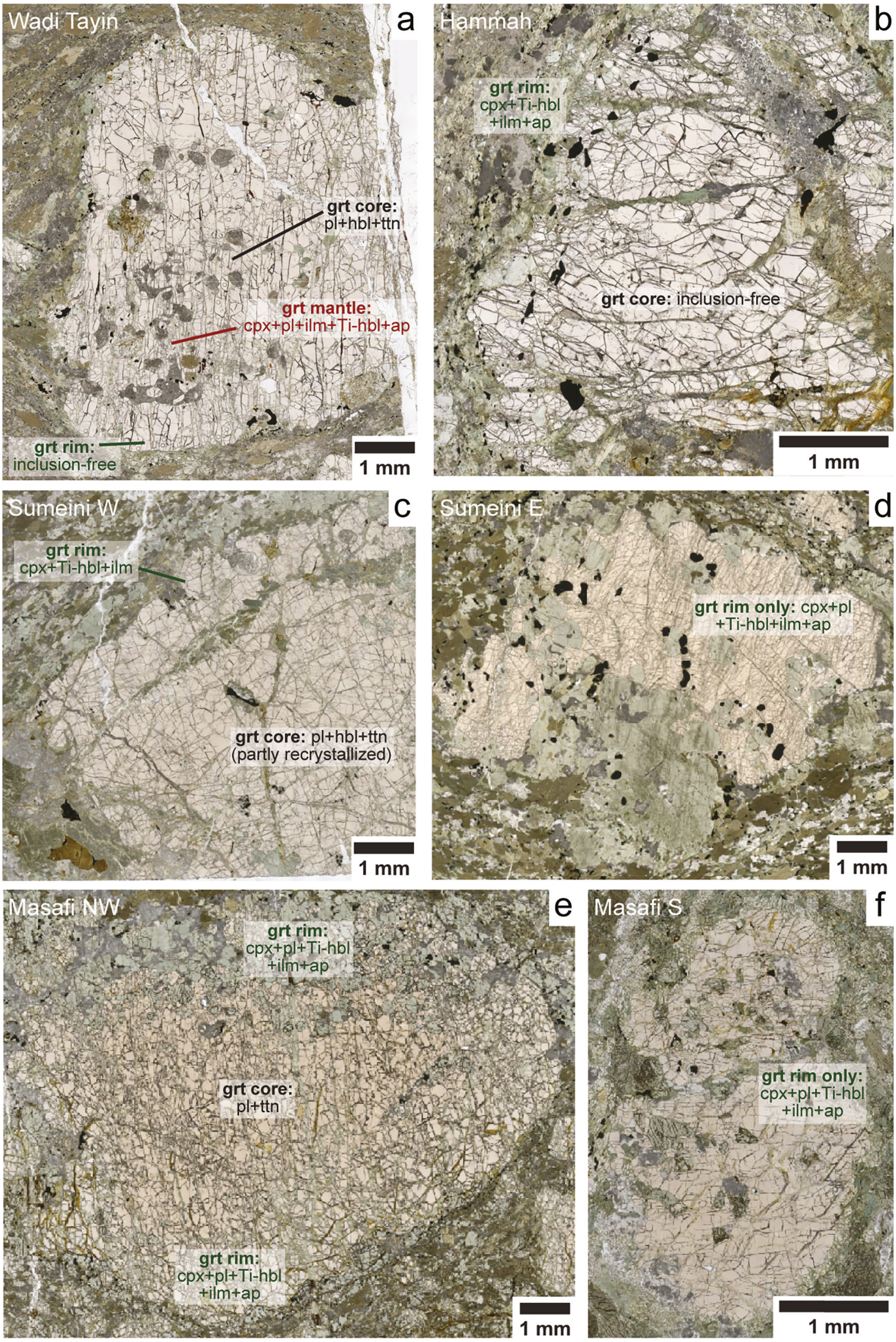

Fig. 2 - Photomicrographs of analysed samples, indicating the range of metamorphic textures observed in garnet-clinopyroxene amphibolites sampled in this study. a) Wadi Tayin (13OJGWT15), showing three different garnet zones and inclusion assemblages (Garber et al., 2025). b) Hammah (171213J02), exhibiting two stages of garnet growth (Garber et al., 2025). c) Sumeini West (171219J05), exhibiting a partly recrystallized, amphibolite-facies garnet core mantled by a granulite-facies garnet rim. d) Sumeini East (171219J03), which includes globular clots dominated by garnet and clinopyroxene that (re)crystallized at granulite-facies conditions and lack amphibolite-facies cores. e) Masafi NW (Wadi Khubakhib; 181219J01), showing a pink, amphibolite-facies garnet core grading to a clear garnet rim with globular, granulite-facies mineral inclusions. f) Masafi S (Asimah Window; 181220J01), showing subhedral garnets with solely granulite-facies inclusions.

0.1–0.6 ε_{Hf} units and <0.1 ε_{Nd} units, demonstrating Hf-Nd isotopic equilibrium among all phases. Additionally, one of these samples underwent Lu-Hf isochron dating (171213J02; Garber et al., 2025), and the isochron $^{176}Hf/^{177}Hfi$ intercept is identical (±0.2 ε_{Hf} units) to that determined from the whole-rock aliquot alone, suggesting the absence of any isotopic disturbance after metamorphism. These data are also compared to previously published zircon ε_{Hf} data (Rioux et al., 2023) from the same samples below. All Nd and Hf isotope data are presented in Table S2.

Laser ablation inductively coupled plasma mass spectrometry (LA-ICPMS) depth profiling of detrital zircon from sample 181212M10 (Al-Ajaiz) was performed at the LionChron facility at The Pennsylvania State University. Zircons were mounted in epoxy with their crystal facets exposed and were not polished prior to analysis. U-Th-Pb isotopes and trace-element data were collected simultaneously from the same spots. Samples were ablated using a Teledyne/Photon Machines Analyte G2 excimer laser ablation system with a Helex2 ablation cell, coupled to a Thermo Scientific Element XR ICPMS system for U-Th-Pb isotopes and a Thermo Scientific iCAP-RQ ICPMS system for trace elements. All elements on both ICPMS systems were measured on secondary electron multipliers. The total Ar gas flow for the experiment was ~2.4 L/min, with total He gas flows from the laser at 0.44 L/min. All analyses were performed in the same session, and all zircons were run with a 25 μm spot size, 10 Hz repetition rate, 250 shots, and a laser fluence at the sample surface of ~4 J/cm2, yielding pit depths on the order of 25 μm. The laser was first fired thrice with the same spot size to remove sample contamination, and this material was allowed to wash out for 20 seconds.

Analyses of unknowns were bracketed by analyses of matrix-matched zircon reference material (RM) 91500 [1062.4±0.4 Ma ID-TIMS $^{206}Pb/^{238}U$ date: (Wiedenbeck et al., 1995)], which was used as the primary RM for U-Pb isotopic analyses. Zircon RMs GJ-1 [601.7±1.3 Ma ID-TIMS $^{206}Pb/^{238}U$ date: (Jackson et al., 2004; Kylander-Clark et al., 2013)], Plešovice [337.13±0.37 Ma ID-TIMS $^{206}Pb/^{238}U$ date: (Sláma et al., 2008)], and Piexe [564±4 Ma ID-TIMS $^{206}Pb/^{238}U$ date: (Dickinson and Gehrels, 2003)] were utilized as secondary RMs, and NIST SRM 612 glass (Jochum et al., 2011) was run as the primary trace-element RM. Using the same parameters and methods applied to unknowns, we obtained U-Pb concordia dates of 597.8±1.3 Ma for GJ-1, 330.1±0.9 Ma for Plešovice, and 566±2 Ma for Piexe during the zircon analytical session, which are accurate to 0.6%, 2.1%, and 0.4% of their reference values, respectively. For trace-element analyses, 29Si (assuming 15 wt. % Si) was used as an internal standard, with measured peaks on the iCAP-RQ at ^{27}Al, ^{29}Si, ^{31}P, ^{45}Sc, ^{49}Ti, ^{89}Y, ^{90}Zr, ^{93}Nb, ^{147}Sm, ^{153}Eu, ^{157}Gd, ^{159}Tb, ^{163}Dy, ^{165}Ho, ^{166}Er, ^{169}Tm, ^{172}Yb, ^{175}Lu, and ^{180}Hf (^{206}Pb, ^{207}Pb, ^{208}Pb, ^{232}Th, and ^{238}U were measured on the Element). Iolite version 4 (Paton et al., 2011) was used to corrected measured isotopic ratios and elemental intensities for baselines, time-dependent laser-induced inter-element fractionation, plasma-induced fractionation, and instrumental drift. The mean and standard error of the measured ratios of the backgrounds and peaks were calculated after rejection of outliers more than two standard errors beyond the mean. Downhole fractionation was modelled using an exponential best fit (Paton et al., 2011). Samples were screened for inclusions using Al and Ti, and discrete cores and rims were identified and selected in Iolite. We added an additional 2% error to each $^{207}Pb/^{235}U$ and $^{206}Pb/^{238}U$ ratio in quadrature to account for variation in ablation or transport characteristics, mass-balance instabilities, or plasma loading effects, which yields a single age population (MSWD≤1) for each of the secondary RMs. Stated 2σ date uncertainties are internal – that is, they include in-run errors only – whereas the long-term external uncertainty for zircon U-Pb in this laboratory is ~2%. IsoplotR (Vermeesch, 2018) was used for all age, concordia, and KDE calculations and plots. The full zircon dataset is contained in Table S3.

RESULTS

Whole rock trace elements

Trace-element data for all sole amphibolites were normalized to chondrite (McDonough and Sun, 1995) and an average normal mid-ocean ridge basalt (N-MORB: Gale et al., 2013, their Table 3); these data are plotted in Fig. 3a-f. The data are compared to the Samail V1 volcanic series (data from Godard et al., 2003; Godard et al., 2006) in Fig. 3g-h. We plotted additional geochemical data from the Haybi Complex further below, using a detailed geochemical study from Haybi rocks in the northern UAE (Dibba Zone: Ziegler et al., 1991b), but there are sparse REE data available for Haybi basalts, hence their absence in Fig. 3. We further calculated REE shape coefficients after O'Neill (2016), which separates the chondrite-normalized REE patterns by average concentration (λ_0), slope (λ_1), parabolic curvature (λ_2), third-order curvature (λ_3), etc. using the BLambdaR program of Anenburg and Williams (2022). These data are displayed in Fig. 3i-k, along with values for average N-MORB and enriched-MORB (E-MORB) basalt endmembers from Gale et al. (2013).

Most samples from south Oman and the UAE, and all samples from Sumeini, exhibit enrichment of LREE relative to HREE, with concave-up, chondrite-normalized patterns and a minor to absent Eu/Eu* anomaly. These samples also exhibit enrichments in Nb, Ta, and LREE relative to N-MORB, while their Zr, Hf, and M-HREE contents are more similar to N-MORB. A subset of samples from south Oman and the UAE sole exposures exhibit concave-down chondrite-normalized patterns with LREE depletion relative to MREE and HREE, and negative Eu/Eu*. These samples also display more N-MORB-like high-field strength (Nb, Ta, Zr, Hf) and REE abundances. All samples exhibit significant Rb, K, Th, Ba, and Sr enrichments relative to N-MORB. In contrast, the V1 trace-element patterns are similar to or more depleted than N-MORB, with pronounced negative Eu/Eu*, and some large-ion-lithophile element enriched outliers. When compared using the REE shape coefficients, all samples scatter between average N-MORB and E-MORB endmembers; those samples with LREE-depleted chondrite-normalized patterns cluster with V1 volcanic samples near the average N-MORB endmember, whereas those samples with LREE-enriched chondrite-normalized patterns approach the E-MORB endmember. Samples from Sumeini plot in the centre of the cluster of sole data, whereas samples from south Oman and the UAE scatter towards both N-MORB and E-MORB endmembers.

The principal components analysis (Fig. 4) provides an additional comparison among all metamorphic sole samples for all elements, including those not plotted in Fig. 3. PC1, the primary axis of variance, discriminates between samples that are relatively LREE, Nb, Ta, and large-ion-lithophile element-rich (negative PC1 score), from those that are more

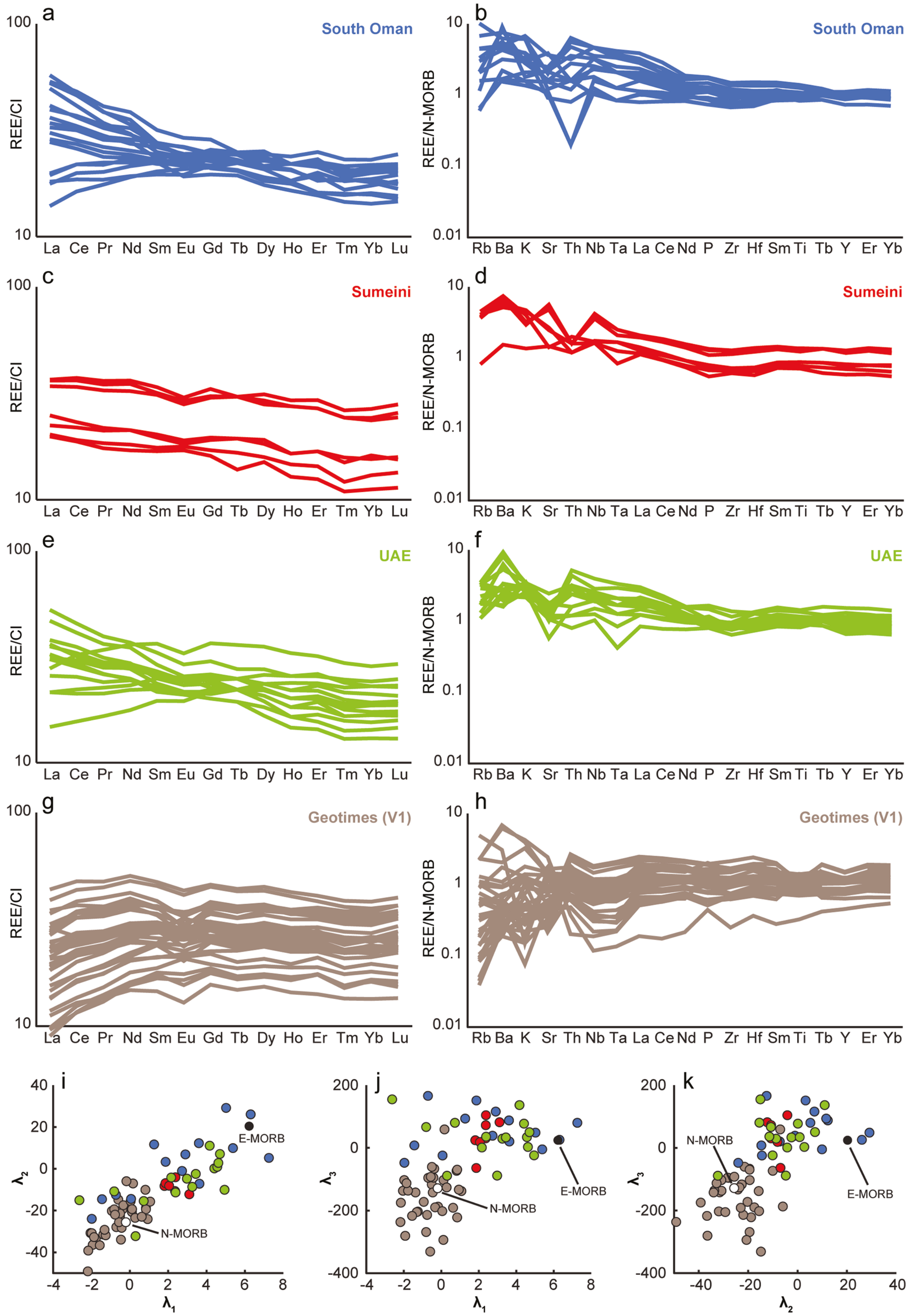

Fig. 3 - Chondrite-normalized rare-earth element (REE) data (a, c, e, g) and N-MORB-normalized trace-element data (b, d, f, h) for sole amphibolite samples from south Oman, Sumeini Window, and the UAE, as well as data from Geotimes (V1) lavas (data from Godard et al., 2003; Godard et al., 2006). Chondrite data for normalization are from McDonough and Sun (1995) and average N-MORB is from Gale et al. (2013). Shape coefficients for the REE data (i-k) were calculated using the method of O'Neill (2016), using the BLambdaR program of Anenburg and Williams (2022); N-MORB and E-MORB endmembers were calculated from the data of Gale et al. (2013).

HREE and transition-metal rich (V, Sc, Co, etc.) (positive PC1 score); the Sumeini samples plot in the centre of this axis whereas south Oman and UAE samples scatter between positive and negative PC1 scores. PC2 discriminates between samples with relative enrichments in REE (particularly MREE) and high-field strength elements (Nb, Ta, Zr, Hf; positive PC2 score) compared to those relatively enriched in all other trace elements (negative PC2 score). The N-MORB vs. E-MORB trends evident in Fig. 3 are somewhat obscured by the PCA compositional normalization; the samples with the most N-MORB-like trace elements plot in the lower-right portion of Fig. 4a. Though it only explains a small proportion of the variance of the dataset, PC3 (Fig. 4b) is useful for identifying three compositionally outlying samples from a single outcrop in Sumeini, with elevated Hg, Sr, Ba, and Rb, whereas the remaining samples cluster together along this axis.

Trace-element ratios were used to consider protolith composition and the possible tectonic setting of the sole amphibolites. These data are plotted in Fig. 5, along with data from Samail V1 basalts (Godard et al., 2003; Godard et al., 2006) and tholeiitic and alkaline basalts from the Haybi Complex (Ziegler et al., 1991b). A plot of Zr/Ti vs. Nb/Y (Winchester and Floyd, 1977; Pearce, 1996), which ties protolith to immobile trace elements rather than major elements that may have been altered (see also Fournier-Roy et al., 2023), is shown in Fig. 5a. Whereas most samples plot at similar Zr/Ti, there is a clear progression with increasing Nb/Y, from Samail V1, to the metamorphic sole and tholeiitic Haybi samples, to the alkaline Haybi samples; the V1, sole, and tholeiitic Haybi plot in the basalt field while the alkaline Haybi rocks plot in the alkaline basalt field. In the V vs. Ti tectonic discrimination diagram (Shervais, 1982) (Fig. 5b), V1, sole, and tholeiitic Haybi samples plot in the MORB or back-arc basalt field, whereas the alkaline Haybi samples plot at significantly higher Ti. Compared to the MORB-ocean island basalt (OIB) array in Th/Yb vs. Ta/Yb space (Pearce, 1983; Pearce, 2008) (Fig. 5c), Samail V1 samples plot around the N-MORB endmember whereas the sole amphibolites plot between E-MORB and N-MORB, with some samples overlapping the V1 basalts (note that there are insufficient Haybi Nb, Ta, Th, and Yb data for comparison). Finally, we compared U/Nb vs. Nb/Zr after John et al. (2004), which is useful for understanding the role of fluid processes during metamorphism (Fig. 5d). Here, Samail V1 exhibits similarities with average N-MORB in Nb/Zr, with U/Nb ranging from average N-MORB to higher values. Sole amphibolites scatter between average N-MORB and E-MORB, but some samples from Sumeini and south Oman have lower U/Nb, and some samples from the UAE scatter to higher U/Nb. Haybi tholeiites exhibit similar Nb/Zr to sole amphibolites, but have markedly higher U/Nb; in contrast, alkaline Haybi basalts plot at significantly higher Nb/Zr values but more modest U/Nb than tholeiitic Haybi basalts.

Whole-rock Nd and Hf isotopes

Nd and Hf isotopic data from a subset of the sole amphibolites are plotted in Fig. 6, with comparison to Samail V1 and V2 (Kusano et al., 2012), Haybi tholeiitic and alkaline basalts (Ziegler et al., 1991b), and zircon ε_{Hf} data from the same samples analysed in this study (Rioux et al., 2023). Data from the sole samples are compared to the mantle Nd-Hf array in Fig. 6a, which show that most sole rocks plot at lower ε_{Nd} and ε_{Hf} than the Samail V1 and other Indian Ocean and East Pacific Rise MORB rocks (e.g., Janney et al., 2005), as well as the bulk of Samail V2 volcanics, although these scatter to significantly lower ε_{Nd}. Notably, one sole sample from the UAE plots within the Samail V1 data.

On an Sm-Nd isochron plot (Fig. 6b), all but one sole sample from this study and all Haybi samples from Ziegler et al. (1991b) plot along a Carboniferous errorchron (352±21 Ma, MSWD = 6), which is within error of the 334±32 Ma errorchron age determined by Ziegler et al. (1991b) from the Haybi samples alone. However, we note that the combined Haybi + sole errorchron is mostly leveraged by the low $^{147}Sm/^{144}Nd$ Haybi samples. The same UAE sole sample that plots within the V1 field in Fig. 6a plots within the Samail V1 Sm-Nd data in Fig. 6b.

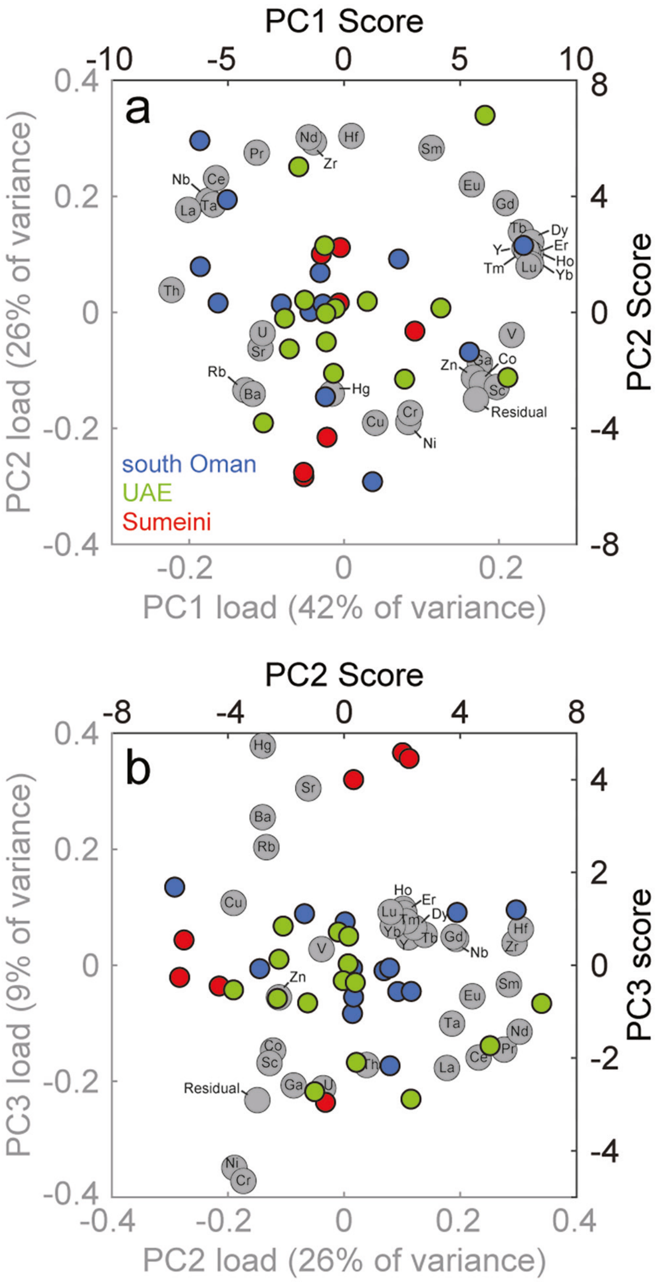

Fig. 4 - Principal components biplots (a: PC1 vs. PC2; b: PC2 vs. PC3) of sole amphibolite trace-element data, with data scores coloured by geographic region (as in Figs. 1-2) and element loadings coloured in gray. The grey loading labeled "Residual" represents an added variable that forces each analysis to sum to 100% (or 1,000,000 ppm), and reflects the influence of unmeasured elements. See text for normalization and method details.

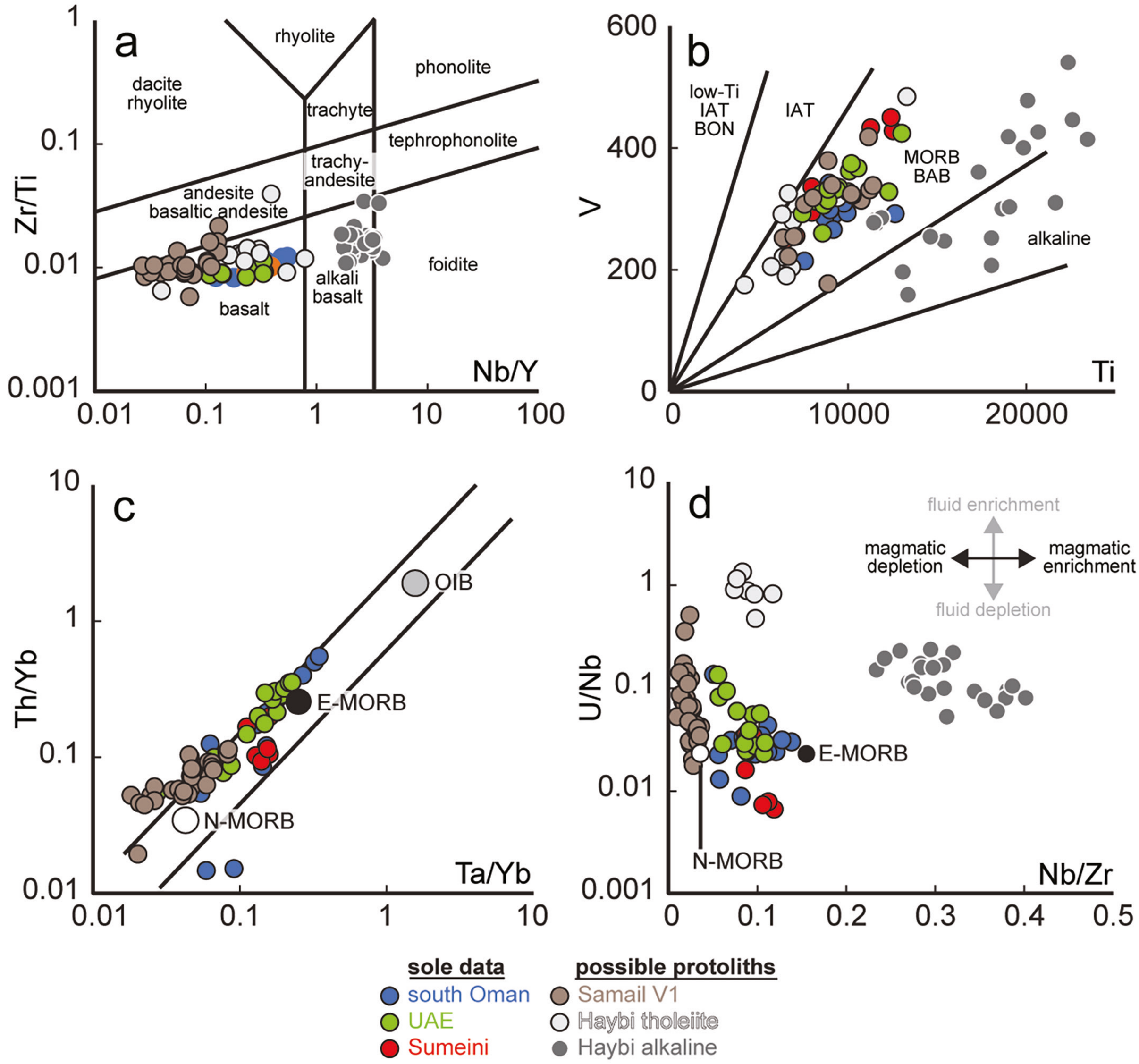

Fig. 5 - Trace-element discrimination plots for sole amphibolites (coloured circles), plotted with data from Samail V1 basalts (in brown; data from Godard et al., 2003; Godard et al., 2006) and tholeiitic (light gray) and alkaline (dark gray) basalts from an exposure of the Haybi Complex in the Dibba Zone, UAE (Ziegler et al., 1991b). a) Zr/Ti vs. Nb/Y plot of Winchester and Floyd (1977), as modified by Pearce (1996). b) V vs. Ti, after Shervais (1982). c) MORB-Ocean Island Basalt (OIB) array in Th/Yb vs. Ta/Yb (Pearce, 1983; Pearce, 2008). d) U/Nb vs. Nb/Zr, after John et al. (2004), with N-MORB and E-MORB endmembers plotted with the data from Gale et al. (2013).

We plotted samples with both whole-rock ε_{Hf} and zircon ε_{Hf} data (the latter determined by Rioux et al., 2023) to understand the relationship between these datasets (Fig. 6c). Although they do not plot along a perfect 1:1 line, all samples are within 2 ε_{Hf} units for both methods, which broadly suggests that the sole zircons reflect the Hf isotopic composition of the rocks they are hosted in, without inheritance or alteration. This observation further indicates that either datum can be used as a proxy for the other for a given sole sample. To understand the coupled temporal-geographic relationship between sole protolith and the timing of metamorphism, Fig. 6d-f shows interrelationships between i) the earliest timing of sole metamorphism as determined by U-Pb zircon dating, using the oldest robust zircon U-Pb date from a given sample (Rioux et al., 2023); ii) the average zircon ε_{Hf} for the sample; and iii) the whole-rock REE patterns (using the chondrite normalized La/Sm ratio). These plots reveal that samples from the Sumeini Window, which contain the oldest metamorphic zircon ages of all sole samples, exhibit the most restricted range of zircon and whole-rock ε_{Hf} values (+9 to +11), and the most reproducible, flat to slightly LREE-rich chondrite-normalized REE patterns (see also Fig. 3). In contrast, samples from south Oman and the UAE exhibit two trends in time-resolved ε_{Hf} and La/Sm space: one trend records a consistent average ε_{Hf} (average of +10) with younging metamorphic age, whereas another projects to significantly higher ε_{Hf} (+13 to +15) over the same time frame. The samples that have more positive ε_{Hf} values also tend to exhibit LREE-depleted, concave-down chondrite-normalized REE patterns. In contrast, the cluster of ε_{Hf}~+10 samples have uniformly LREE-rich, concave-up chondrite-normalized REE. Strikingly, even though this average ε_{Hf} value for the majority of the sole amphibolites does not vary with younging metamorphic age, the maximum whole-rock La/Sm value shows significant variation for the same samples, from ~1 in Sumeini, to ~1.5 in samples from the UAE, to ~2 in samples from south Oman.

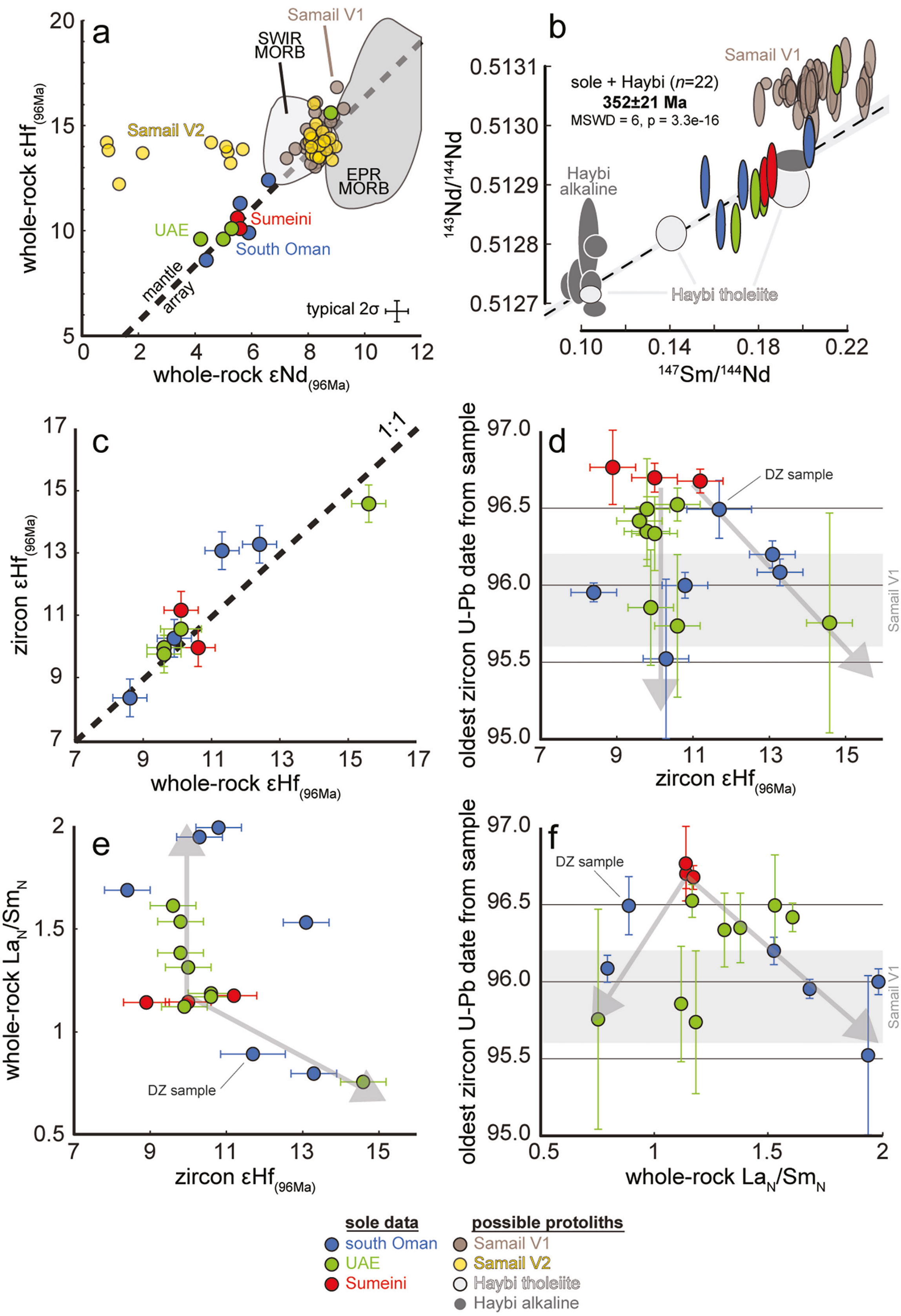

Fig. 6 - Hf and Nd isotope data, including new whole-rock data from this study (coloured circles and error ellipses in a, b, and c), published Samail V1 (brown) and V2 (yellow) whole-rock basalt data (Kusano et al., 2012), published Haybi Complex alkaline (dark gray) and tholeiitic (light gray) basalt data (Ziegler et al., 1991b), and published zircon U-Pb and εHf data from the same rocks analysed in this study (Rioux et al., 2023; data in d, e, and f). a) Hf-Nd isotope mantle array, with data from the southwest Indian Ocean ridge and East Pacific Rise from Janney et al. (2005 and references therein). b) Sm-Nd isochron plot. c) Comparison between whole-rock and zircon εHf data analysed on the same samples. d) Zircon U-Pb date vs. zircon εHf for sole amphibolites, relative to the timing of Samail V1 (Rioux et al., 2012; Rioux et al., 2013). e) Whole rock, chondrite-normalized La/Sm vs. zircon εHf for sole amphibolites. f) Zircon U-Pb date vs. whole-rock, chondrite-normalized La/Sm.

Zircon U-Pb and trace-element data

Sample 181212M10, from Al-Ajaiz in southern Oman, was previously identified (Rioux et al., 2023) to contain inherited detrital zircons, in addition to a metamorphic population of zircons dated at 96 Ma; we analysed zircons from the same crushed rock samples as in the previous study. These samples were depth profiled to recover both zircon rim and core information. The U-Pb data (colored by Th/U) are plotted in Fig. 7a, with a closeup of the youngest data plotted in Fig. 7b. The data scatter from ~2400–96 Ma, with a textural control on the resulting dates. For example, all zircons with ~96 Ma dates are from discrete grains (also noted in Rioux et al., 2023), although these are not easily discernible from the remaining detrital zircon population. All ages older than ~400 Ma are from the cores of zircon grains, but there is a discrete age population at ~300 Ma that only occurs as metamorphic rims on igneous cores with ages from ~550–1400 Ma. In trace-element plots (Eu/Eu*, Dy/Yb, and Th/U: Fig. 7c-e), these rims are clearly distinct, with a less negative Eu anomaly, more depleted HREE, and significantly lower Th/U. A kernel density plot indicates several significant age peaks, including 2010, 1721, 1468, 1190, 1089, 598, and 299 Ma, with the latter of these entirely defined by the zircon rims (Fig. 7f).

DISCUSSION

Composition of sole protoliths

All garnet-clinopyroxene sole amphibolites are consistent with basaltic protoliths: i) they have relatively fine-grained retrograde amphibole-plagioclase dominated matrices with large, prograde to peak garnet-clinopyroxene clots (Fig. 2); ii) they have trace-element patterns and concentrations consistent with those expected for MORB-like, basaltic protoliths (Fig. 3, 5a-5c); iii) they lack positive Eu anomalies that would indicate magmatic plagioclase accumulation (Fig. 3); and iv) they have Nd and Hf isotopic compositions that plot along the mantle array (Fig. 6a). The analyzed garnet-clinopyroxene sole amphibolites also exhibit elevated concentrations of fluid-mobile and large-ion-lithophile elements such as Rb, Ba, and K (Fig. 3) consistent with significant fluid alteration from fluid flow along the sole thrust (Yoshikawa et al., 2015; Ambrose et al., 2018; Prigent et al., 2018; Searle et al., 2022), or from structurally lower metabasalts (e.g., Ishikawa et al., 2005). Variations in these and other fluid-mobile elements (Figs. 3, 4, 5d) suggest variable metasomatic intensity among sole exposures, which is particularly notable in a subset of metabasalts from Sumeini rich in Hg, Sr, Ba, and Rb (i.e., fluid-mobile elements; Fig. 4b).

Even considering the effects of elemental mobility during metamorphism, there are variations in basaltic protolith that are identified using the most lithophile, immobile trace elements, as well as Nd and Hf isotopes. Though samples generally plot on a trend line between endmembers, the data identify two basaltic protoliths for sole amphibolites: a dominant endmember that is more similar to average E-MORB (which was also identified by Ishikawa et al., 2005; Kim et al., 2020), and a subsidiary endmember that is more like average N-MORB. The E-MORB metabasalts are geographically widespread, and are defined by concave-up chondrite-normalized REE patterns, elevated Nb and Ta relative to Zr and Hf, elevated Th/Yb and Ta/Yb, and less positive ε_{Nd} and ε_{Hf}. In contrast, the N-MORB endmember is defined by concave-down to hump-shaped chondrite-normalized REE patterns, Nb-Ta-Zr-Hf concentrations similar to N-MORB, lower Th/Yb and Ta/Yb, and more positive ε_{Nd} and ε_{Hf}. Notably, whereas any one sole outcrop appears to tend toward either the E-MORB or N-MORB endmember, and while the earliest metamorphosed Sumeini Window sole protolith appears relatively homogeneous, analyses across multiple adjacent outcrops in south Oman and the UAE shows that these distinct protoliths are intercalated on a 5–10 km scale (Fig. 1).

The E-MORB geochemical trend is nominally consistent with the tholeiitic basalts of the Haybi Complex. For most trace-element and isotopic comparisons, the E-MORB sole endmember and Haybi tholeiites are either indistinguishable (Fig. 5a-b), share a plausible genetic relationship (Fig. 6b), or have differences that can be explained by metamorphic or metasomatic effects (Fig. 5d). Rocks of the Haybi Complex have long been considered the most plausible sole protolith given their position in the thrust sheet immediately below the sole, the abundance of basalts in the Haybi Complex, and the intercalation of basalts and carbonates that is also observed at sole outcrops like the Sumeini Window (Searle and Malpas, 1980; Searle and Graham, 1982; Searle and Malpas, 1982; Searle and Cox, 2002). Though the stratigraphically higher tholeiitic basalt member of the Haybi Complex is thinner than the lower alkaline basalt unit (Searle and Cox, 2002), the absence of alkaline basalt protoliths in the sole suggests that the tholeiites may have been more abundant further outboard of the continental margin, where the Samail subduction zone initiated. Despite the similarities between sole amphibolites and Haybi Complex tholeiites, one observation that remains unexplained is the differences in whole-rock La/Sm between different geographic locations (e.g., Fig. 6f), with samples from south Oman and the UAE characterized by more significant LREE enrichments compared to similar metabasalts in the Haybi Complex, despite all of them exhibiting similar ε_{Nd} and ε_{Hf} values. The PCA (Fig. 4) demonstrates that these variable LREE enrichments are correlated with variations in several other elements, including high-field strength elements and transition metals. It is therefore likely that this compositional diversity represents initial geographic variability in Haybi Complex basaltic protoliths, which is as yet unconstrained but can be readily tested on exposed, unmetamorphosed Haybi Complex samples. On the other hand, with the current dataset, we cannot rule out that some of this variability in the E-MORB-like sole amphibolites was caused by later metasomatism.

The N-MORB basalt trend has not previously been reported for the highest-grade garnet-clinopyroxene sole amphibolites, although Ishikawa et al. (2005) noted a similar N-MORB-like whole-rock trace-element pattern for lower-grade amphibolites from Wadi Tayin in south Oman. The occurrence of km-scale variations in N-MORB and E-MORB sole compositions provides three possible protolith options. First, although there have been no basalts reported from the Haybi Complex with N-MORB-like compositions, these may have been emplaced only in the most outboard, distal portions of the Haybi Complex (Fig. 8, Model 1). The apparent absence of N-MORB basalts in the exposed Haybi Complex protolith, however, permits that a heterogeneous section of Indian Ocean MORB crust unrelated to the Haybi may have been the protolith for all sole amphibolites (Fig. 8, Model 2). It is widely recognized that mid-ocean ridge segments exhibit heterogeneous elemental and isotopic compositions between depleted (D-)MORB and E-MORB at the spatial scale observed in this study (Perfit et al., 1994; Niu et al., 1999;

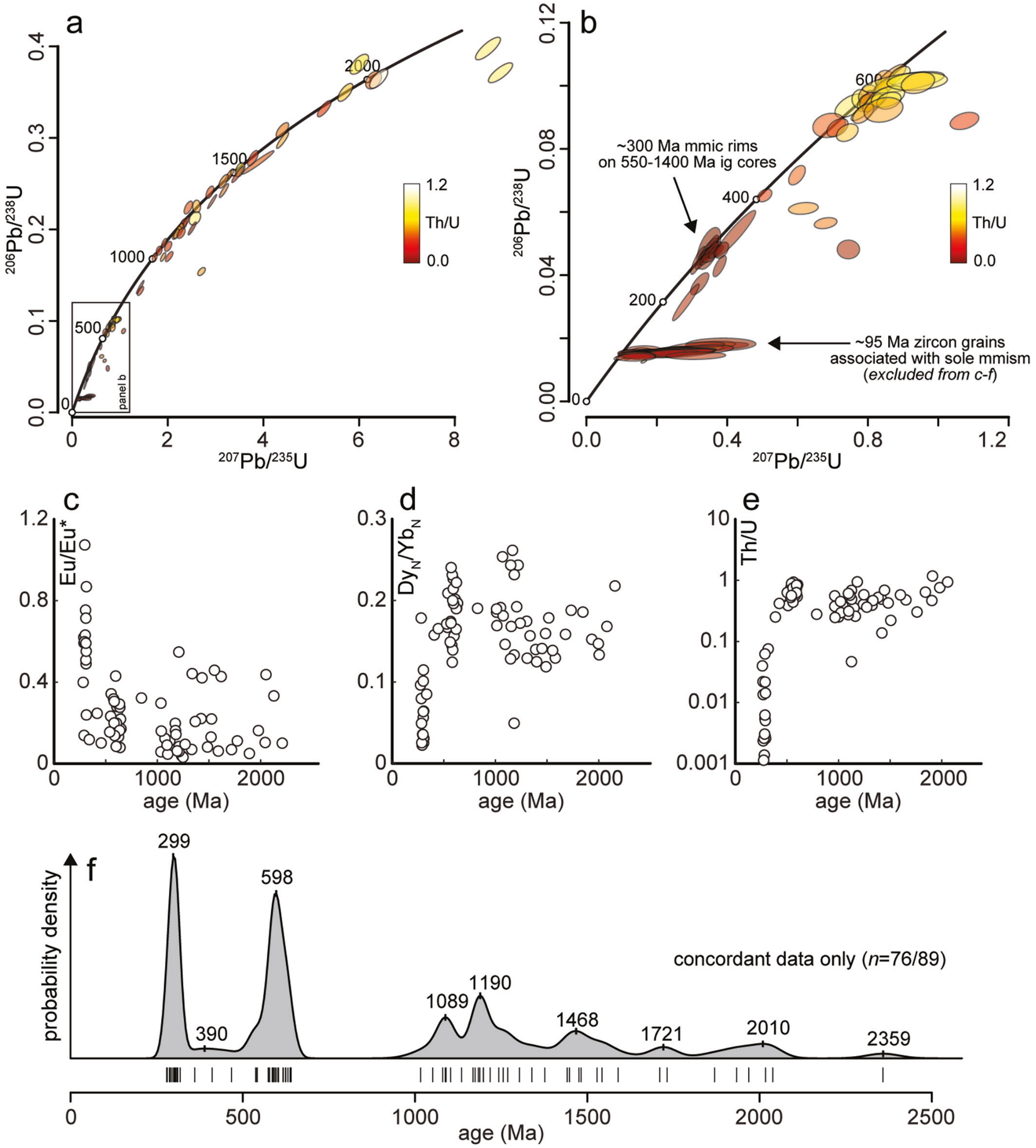

Fig. 7 - Detrital zircon age and trace-element data from sample 181212M10 (Al-Ajaiz). a) Wetherill concordia plot of all detrital zircon U-Pb data, coloured by Th/U. b) Inset of panel a, showing three main young zircon populations, including the main metamorphic population at ~95 Ma. c) Eu/Eu*, d) chondrite-normalized Dy/Yb, and e) Th/U for the detrital zircon data. f) Kernel density estimate (KDE) calculated in IsoPlotR (Vermeesch, 2018) for concordant U-Pb zircon data, with identified significant age peaks.

Waters et al., 2011), including in the ~135 Ma Masirah Ophiolite in southeastern Oman, where variable compositions even occur at the meter scale (Jansen et al., 2024). These chemical heterogeneities are thought to relate to differences in mantle source, i.e., melts of recycled MORB pyroxenites for E-MORB and depleted peridotites for D-MORB (Prinzhofer et al., 1989; Niu et al., 1999; Yang et al., 2020). Based on a compilation of global MORB data, Jansen et al. (2024) noted that the presence of MORB chemical heterogeneity is more common at slower-spreading ridges likely due to lower melt fractions, although it is also observed at several fast-spreading ridges (e.g., the East Pacific Rise).

A final possible source for the rarer N-MORB basaltic protoliths is the Samail V1 volcanic series (Fig. 8, Model 3).

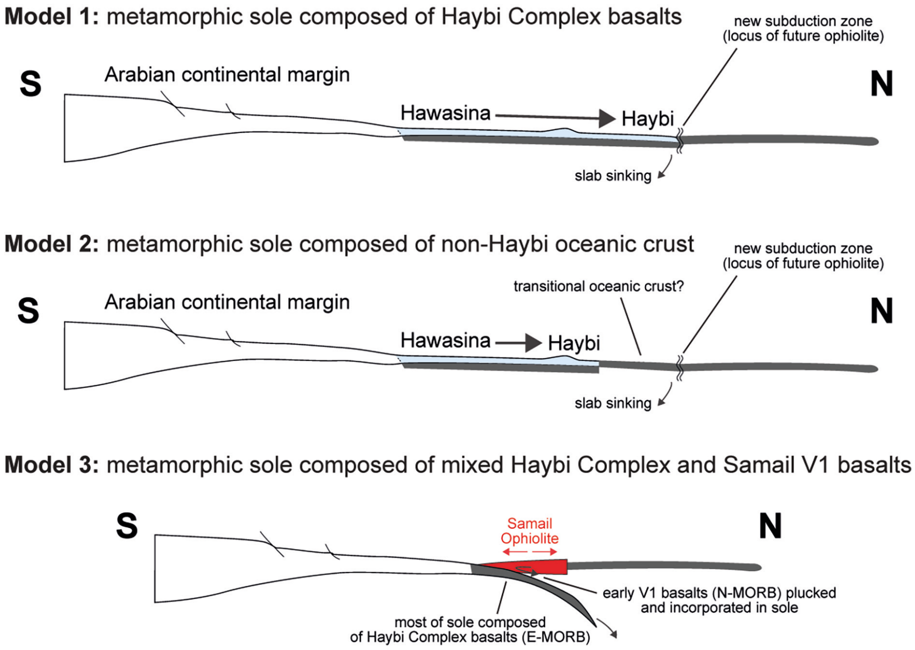

Fig. 8 - Tectonic cartoon indicating the three possible protolith models for the Samail metamorphic sole. Model 1 represents the case in which the Haybi Complex forms the entirety of the metamorphic sole, which would place Haybi Complex basalts at the locus of the newly-developing Samail subduction zone. Model 2 reflects the influence of non-Haybi Complex basaltic oceanic crust in forming the metamorphic sole, which would require a suture between the Haybi Complex and this oceanic crust outboard of the former Arabian continental margin. Model 3 represents the case in which the N-MORB-like sole metabasalt protoliths were derived from nascent Samail Ophiolite V1 basalts, mixed with E-MORB-like protoliths derived from the Haybi Complex. Because the Sumeini Window contains the earliest sole metamorphic ages and the most homogeneous, E-MORB-like protoliths, this model still requires either Haybi Complex or other E-MORB oceanic crust to have formed the initial portion of the metamorphic sole.

In particular, the consistency in immobile trace-element (Fig. 3, Fig. 5a-c) and Nd-Hf isotopes (Fig. 6a-b) between Samail V1 and the most N-MORB-like sole amphibolites analysed herein provide circumstantial evidence for their derivation from the Samail V1 series. There are, however, several points of caution in this interpretation. First, only a few samples exhibit unequivocal N-MORB character in both trace elements and isotopes, which would require that intermediate samples (e.g., Fig. 5c-d) represent physical mixtures between E-MORB (e.g., Haybi) and V1 (N-MORB) protoliths. More importantly, given the geochronology of the ophiolite and sole, there are timing issues with having Samail V1 basalts sensu stricto in the metamorphic sole. Considering a maximum convergence rate of ~30 km/Myr (Agard et al., 2007), metamorphic pressures of 1.0-1.5 GPa for garnet-clinopyroxene amphibolites (Gnos, 1998; Cowan et al., 2014; Soret et al., 2017) corresponding to depths of ~30-40 km if pressure was lithostatic, and considering a wide range of dip angles (15-60ºC), a V1 basalt that was incorporated into the sole would have had to start subducting 1-4 Myr prior to the timing of metamorphism. Because the earliest prograde to peak metamorphic dates for sole zircons from "V1-like" samples are ~96.2 Ma, that would require V1 basalts to have started erupting by ~97-98 Ma – earlier than the earliest timing of V1 magmatism preserved in the ophiolite (96.2-95.6 Ma). There are considerations that may mitigate these issues; for example, convergence or plate sinking rates may locally have been higher than the broader Arabia-Eurasia convergence rate, especially considering that ophiolite spreading rates were up to 100 mm/yr (Rioux et al., 2012), and metamorphic pressures in the sole may not have been lithostatic (e.g., Garber et al., 2020). Additionally, although it has been contested (Valera et al., 2026), Keenan et al. (2016) suggested similar ~1 Myr timescales in the Palawan Ophiolite (Philippines) between protolith basalt crystallization at an ocean ridge, and sole metamorphism at depth. It is also possible that the magmatic rocks now preserved in the ophiolite may not represent the entire original extent of newly crystallized oceanic crust, and because the oldest robust sole metamorphic dates are ~96.7 Ma (Rioux et al., 2023), there may have been older pieces of ophiolite crust that were not preserved during or after obduction. Ultimately, while we cannot rule out that some basalts may have had V1 protoliths, we find this option the least plausible, and suggest that the Haybi Complex or an unrelated Indian Ocean MORB protolith are most likely.

We also note that there are downsection variations in sole geochemistry within each sole exposure that are not investigated here, which will likely clarify the time-resolved evolution of sole protoliths. Ishikawa et al. (2005) identified a transition from garnet- and clinopyroxene-bearing, E-MORB-like metabasalts at the top of the Wadi Tayin section, grading downwards to garnet-free V1 and V2-like metabasalts at the base of the section with intercalated cherts. Subsequent geochronology of detrital zircons in the structurally highest chert layer at Wadi Tayin showed detrital zircons as young as ~105 Ma (Garber et al., 2020). Similar differences between DZ ages and ophiolite crystallization ages were found for metasediments in the Ordovician Bay of Islands Ophiolite by Fournier-Roy et al. (2023), indicating that despite possibly older protolith ages for the basalts themselves, the rocks now constituting these soles were probably exposed at the seafloor until shortly prior to emplacement.

Finally, the ε_{Nd} and ε_{Hf} data presented here have bearing on the timing of Samail sole metamorphism, discussed above. The main controversy revolves around whether the sole rocks reached peak metamorphism nearly synchronously with the overlying ophiolite at ~96.7–94.7 Ma (based on zircon U-Pb dates and trace-element concentrations: Rioux et al., 2016; Rioux et al., 2023), or significantly before ophiolite formation at ~104 Ma (based on garnet-whole rock Lu-Hf isochron dates: Guilmette et al., 2018). In presenting a new, significantly younger sole garnet-zircon-whole rock Lu-Hf date of 97.9±0.5 Ma, Garber et al. (2025) noted that the previously published dates from Guilmette et al. (2018) yielded ε_{Hf} intercepts that were far lower (-5 to -11) than any previously published Hf isotopic data from the sole, which at that time was limited to the zircon ε_{Hf} data of Rioux et al. (2023). Here, we show that nearly all sole metabasalts have high ε_{Hf} (+9 to +15); that all whole-rock digestion methods yield the same result within uncertainty; that whole-rock and zircon data agree within 2 ε_{Hf} units; and that the ε_{Nd} and ε_{Hf} data are internally consistent, lying along the mantle array. These observations again emphasize that the older Lu-Hf dates for sole metamorphism are unsupported. Importantly, other soles (from other ophiolites) dated by the Lu-Hf method – with garnet isochron dates significantly older than zircon U-Pb dates from the same rocks – also result in geologically unreasonable initial Hf isotopic compositions (Guilmette et al., 2023) that do not match zircon ε_{Hf} from the same outcrops (Shen et al., 2025), and therefore should be viewed with caution.

Age of sole protoliths

The presence of detrital zircons in sample 181212M10 is fortuitous, and because exclusively metamorphic (~96 Ma) zircons from this sample have a modest ε_{Hf} value (+11.7±0.9: Rioux et al., 2023) matching other E-MORB/Haybi-like sole samples (e.g., Fig. 6), the sample presents a unique opportunity to understand the maximum depositional age and tectonic setting of many of the sole protoliths as well as the Haybi Complex. Indeed, the only existing geochronological data for the Haybi Complex basalts are biotite K/Ar ages spanning ~230–200 Ma (Searle et al., 1980; Lippard and Rex, 1982).

Many of the detrital age peaks in 181212M10 (Fig. 7f) are consistent with derivation from the Arabian Plate. For example, pan African (550-650 Ma) age peaks associated with Gondwana assembly are common throughout the Arabian-Nubian Shield (Stern and Johnson, 2010; Robinson et al., 2014; Gamaleldien et al., 2022), and most of the remaining age peaks (~1.0–1.2, ~1.7, ~2.0, and ~2.4 Ga) are found in other regional detrital zircon suites (Avigad et al., 2003; Stern and Johnson, 2010; Meinhold et al., 2021; Gómez-Pérez et al., 2024) or as xenocrystic zircons in Arabian-Nubian Shield volcanic and plutonic rocks (Stern et al., 2010), suggesting common provenance with other nearby rock suites. The 1.4-1.5 Ga age peak in sample 181212M10 is notably rare in other regional detrital zircon data, but zircons with similar dates were recently reported from the late Ediacaran Ara clastics in southern Oman (Gómez-Pérez et al., 2024) as well as the Cretaceous Muti Formation in northern Oman (Ahmed Abbasi et al., 2026), suggesting that source lithologies of this age were exposed to weathering in the Arabian Shield at the time of Haybi emplacement.

In contrast, ~299 Ma zircon rims have trace-element compositions that are distinct from all zircon cores (lower Th/U and Dy/Yb, higher Eu/Eu*) (Fig. 7c-e). In particular, the significantly lower Th/U for these rims suggest that they represent metamorphic zircon (re)crystallization rather than igneous growth (Yakymchuk et al., 2018). Because not all zircons exhibit these rims, it is unlikely that the entire rock was metamorphosed at ~299 Ma prior to being incorporated into the metamorphic sole, but rather that this represents a metamorphic event that variably affected the source rocks that eroded to form the (now) metasediment. Interestingly, this date roughly matches the timing of volcanism along a pre-Permian stratigraphic unconformity preserved throughout northern Oman, based on zircon U-Pb dates from felsic volcanics in the eclogite-facies As Sifah Unit (298-284 Ma: Gray et al., 2005; Garber et al., 2021). This unconformity – and the volcanism associated with it – likely relates to the initiation of intracontinental rifting; although the timing of rifting is debated and may have been diachronous across the Arabian margin, it is generally agreed that rift basins and rift-related magmatism (including the Haybi Complex) were widespread by 270–260 Ma (Chauvet et al., 2009 and references therein), providing a maximum age for the timing of eruption of Haybi-like sole protoliths. We also note the presence of a Carboniferous Sm-Nd errorchron for the combined Haybi-sole samples (352±21 Ma: Fig. 6b) which nominally suggests an older potential emplacement age for the Haybi Complex. However, because this age is older than the detrital zircons contained within a Haybi-like sole amphibolite, and also significantly pre-dates the timing of rifting in Oman, we are skeptical that this age is geologically meaningful (similar to the conclusions of Ziegler et al., 1991b). Nevertheless, the isotopic consanguinity between Haybi and E-MORB-like sole samples provides further confidence that these suites are related.

The age of potential non-Haybi, Indian Ocean MORB protoliths for the sole is more tenuous. Based on global plate tectonic reconstructions (Seton et al., 2012), the age of oceanic crust located offshore of Oman during ophiolite crystallization at 96 Ma was 100-140 Myr (i.e., 200–240 Ma at present), providing a maximum age for other oceanic crustal protoliths.

Implications for tectonic and thermal models of Samail Ophiolite formation

The results presented here have implications for understanding the formation of the Samail Ophiolite. One challenge for modelling ophiolite emplacement is the paucity of constraints on the protolith ages of the metamorphic sole. Here, the connection between the Haybi Complex and most sole protoliths, as well as the age constraints provided by detrital zircons, suggests that the Samail lower plate was ≥150 Ma at the time of subduction initiation, which matches the boundary conditions assumed in several thermal models (e.g., Duretz et al., 2016). Although there are protoliths within the Samail sole that could plausibly relate to the Samail V1 volcanic suite, the preservation of E-MORB signatures in the earliest metamorphosed basalts, and the general dominance of E-MORB signatures in sole amphibolites, makes it difficult to support models for Samail subduction initiation at a newly-formed mid-ocean ridge (Boudier et al., 1988).

On the other hand, if the Samail V1 volcanics are the protolith for the N-MORB-like sole amphibolites, this would present a unique thermal problem, because all garnet-clinopyroxene sole amphibolites throughout the entire Samail sole have nearly identical P-T conditions. The resulting absence of a connection between lower-plate age and peak sole metamorphic temperature is curious, as a thermal relationship should be expected if heating of the sole was conductive from the overlying ophiolite mantle section (as for subduction zones: Syracuse et al., 2010; Penniston-Dorland et al., 2015). The range of peak P-T conditions for worldwide metamorphic soles throughout geologic history is relatively narrow (Agard et al., 2016), suggesting the absence of an age-temperature connection among different ophiolites; the data presented in this study may suggest the absence of this correlation within a single ophiolite.

Finally, the presence of spatially resolved changes in sole protolith indicates that the nature of the lower plate was not uniform prior to subduction, with each geographic segment displaying unique characteristics. For example, whereas the isotopic character of the E-MORB sole endmember appears relatively constant over the total interval of sole metamorphism, both E-MORB and N-MORB endmembers are heterogeneous with respect to trace elements, with both south Oman and the UAE deviating to higher and lower trace-element abundances with time from an "average" sole composition represented by the earliest metamorphosed sole exposures in the Sumeini Window. It is also worth noting that soles with peak metamorphic ages deviating by up to ~1 Myr occur adjacent to each other (Rioux et al., 2023). These observations suggest that – despite regional and even global similarities in sole P-T conditions and protolith trends – sole formation also reflects a suite of highly localized processes.

CONCLUSIONS

New geochemical data from the Samail metamorphic sole reveal the presence of chemically heterogeneous protoliths for the highest-grade, garnet-clinopyroxene amphibolites. An E-MORB-like endmember occurs regionally throughout the Samail massif, and has numerous isotopic and trace-element similarities with tholeiitic basalts from the Permo-Triassic portion of the Haybi Complex, which represents the structurally highest unmetamorphosed thrust sheet beneath the metamorphic rocks of the sole. One sample of this protolith contains detrital zircons with ~299 Ma metamorphic rims, providing a maximum depositional age for these sole rocks. A less abundant N-MORB-like endmember only occurs within south Oman and the UAE. It is unclear whether 1) this protolith represents an unidentified member of the Haybi Complex, 2) both protoliths occurred together in Permian to Triassic Indian Ocean MORB unrelated to the Haybi Complex, or 3) the N-MORB protolith represents some underthrusted sections of the Samail V1 volcanic suite; options (1) and (2) are most plausible, but (3) cannot be ruled out.

ACKNOWLEDGEMENTS

We thank the Director General of Minerals, Ministry of Commerce and Industry of the Sultanate of Oman for allowing us to conduct fieldwork in the Sultanate of Oman. We are grateful to Stan Mertzman for performing the XRF measurements. We appreciate the thorough and helpful comments provided by two anonymous reviewers, as well as editorial handling by Daniele Brunelli. This research was supported by National Science Foundation grant EAR-2120931 to J.M.G. and A.J.S., National Science Foundation grants EAR-1250522 and EAR-1650407 to M.R., and The Pennsylvania State University.

ONLINE SUPPLEMENTARY MATERIAL

Supplementary data to this article are available online at https://doi.org/10.4454/ofioliti.v51i2.587

REFERENCES

Agard P., Jolivet L., Vrielynck B., Burov E. and Monié P., 2007. Plate acceleration: The obduction trigger? Earth Planet. Sci. Lett., 258: 428-441. https://doi.org/10.1016/j.epsl.2007.04.002

Agard P., Yamato P., Soret M., Prigent C., Guillot S., Plunder A., Dubacq B., Chauvet A. and Monié P., 2016. Plate interface rheological switches during subduction infancy: Control on slab penetration and metamorphic sole formation. Earth Planet. Sci. Lett., 451: 208-220. http://dx.doi.org/10.1016/j.epsl.2016.06.054

Ahmed Abbasi I., Qasim M., Attar J.A., El-Ghali M.A.K., Moustafa M.S.H. and Ding L., 2026. Detrital Zircon U–Pb Geochronology of the Muti Formation: Implications for Provenance and Evolution of the Oman Foreland Basin. Geosciences, 16: 15. https://doi.org/10.3390/geosciences16010015

Aitchison J., 1982. The Statistical Analysis of Compositional Data. J. Royal Stat. Soc. Series B (Methodological), 44: 139-177. https://doi.org/10.1111/j.2517-6161.1982.tb01195.x

Alabaster T., Pearce J.A. and Malpas J., 1982. The volcanic stratigraphy and petrogenesis of the Oman ophiolite complex. Contrib. Mineral. Petrol., 81: 168-183. https://doi.org/10.1007/bf00371294

Ambrose T.K., Wallis D., Hansen L.N., Waters D.J. and Searle M.P., 2018. Controls on the rheological properties of peridotite at a palaeosubduction interface: A transect across the base of the Oman–UAE ophiolite. Earth Planet. Sci. Lett., 491: 193-206. https://doi.org/10.1016/j.epsl.2018.03.027

Ambrose T.K., Waters D.J., Searle M.P., Gopon P. and Forshaw J.B., 2021. Burial, Accretion, and Exhumation of the Metamorphic Sole of the Oman-UAE Ophiolite. Tectonics, 40: e2020TC006392. https://doi.org/10.1029/2020TC006392

Anenburg M. and Williams M.J., 2022. Quantifying the Tetrad Effect, Shape Components, and Ce–Eu–Gd Anomalies in Rare Earth Element Patterns. Mathem.Geosci., 54: 47-70. https://doi.org/10.1007/s11004-021-09959-5

Avigad D., Kolodner K., McWilliams M., Persing H. and Weissbrod T., 2003. Origin of northern Gondwana Cambrian sandstone revealed by detrital zircon SHRIMP dating. Geology, 31: 227-230. https://doi.org/10.1130/0091-7613(2003)031<0227:Oongcs>2.0.Co;2

Belgrano T.M. and Diamond L.W., 2019. Subduction-zone contributions to axial volcanism in the Oman–U.A.E. ophiolite. Lithosphere, 11: 399-411. https://doi.org/10.1130/l11045.1

Belgrano T.M., Diamond L.W., Vogt Y., Biedermann A.R., Gilgen S.A. and Al-Tobi K., 2019. A revised map of volcanic units in the Oman ophiolite: insights into the architecture of an oceanic proto-arc volcanic sequence. Solid Earth, 10: 1181-1217. https://doi.org/10.5194/se-10-1181-2019

Boudier F., Ceuleneer G. and Nicolas A., 1988. Shear zones, thrusts and related magmatism in the Oman ophiolite: Initiation of thrusting on an oceanic ridge. Tectonophysics, 151: 275-296. https://doi.org/10.1016/0040-1951(88)90249-1

Bouvier A., Vervoort J.D. and Patchett P.J., 2008. The Lu–Hf and Sm–Nd isotopic composition of CHUR: Constraints from unequilibrated chondrites and implications for the bulk composition of terrestrial planets. Earth Planet. Sci. Lett., 273: 48-57. http://dx.doi.org/10.1016/j.epsl.2008.06.010

Carosi R., Cortesogno L., Gaggero L. and Marroni M., 1996. Geological and Petrological Features of the Metamorphic Sole From the Mirdita Nappe, Northern Albania. Ofioliti, 21: 21-40.

Chauvet F., Dumont T. and Basile C., 2009. Structures and timing of Permian rifting in the central Oman Mountains (Saih Hatat). Tectonophysics, 475: 563-574. https://doi.org/10.1016/j.tecto.2009.07.008

Cluzel D., Jourdan F., Meffre S., Maurizot P. and Lesimple S., 2012. The metamorphic sole of New Caledonia ophiolite: $^{40}Ar/^{39}Ar$, U-Pb, and geochemical evidence for subduction inception at a spreading ridge. Tectonics, 31. https://doi.org/10.1029/2011TC003085

Cowan R.J., Searle M.P. and Waters D.J., 2014. Structure of the metamorphic sole to the Oman Ophiolite, Sumeini Window and Wadi Tayyin: implications for ophiolite obduction processes. Geol. Soc. London, Spec. Publ., 392: 155-175. https://doi.org/10.1144/SP392.8

Dewey J.F. and Casey J.F., 2013. The sole of an ophiolite: the Ordovician Bay of Islands Complex, Newfoundland. J. Geol. Soc., 170: 715-722. https://doi.org/10.1144/jgs2013-017

Dickinson W.R. and Gehrels G.E., 2003. U–Pb ages of detrital zircons from Permian and Jurassic eolian sandstones of the Colorado Plateau, USA: paleogeographic implications. Sedim. Geol., 163: 29-66. https://doi.org/10.1016/S0037-0738(03)00158-1

Dilek Y. and Furnes H., 2014. Ophiolites and Their Origins. Elements, 10: 93-100. https://doi.org/10.2113/gselements.10.2.93

Dimo-Lahitte A., Monié P. and Vergély P., 2001. Metamorphic soles from the Albanian ophiolites: Petrology, $^{40}Ar/^{39}Ar$ geochronology, and geodynamic evolution. Tectonics, 20: 78-96. https://doi.org/10.1029/2000TC900024

Duretz T., Agard P., Yamato P., Ducassou C., Burov E.B. and Gerya T.V., 2016. Thermo-mechanical modeling of the obduction process based on the Oman Ophiolite case. Gondwana Res., 32: 1-10. https://doi.org/10.1016/j.gr.2015.02.002

Farahat E.S., 2011. Geotectonic significance of Neoproterozoic amphibolites from the Central Eastern Desert of Egypt: A possible dismembered sub-ophiolitic metamorphic sole. Lithos, 125: 781-794. https://doi.org/10.1016/j.lithos.2011.04.009

Fournier-Roy F., Guilmette C., Larson K., Godet A., Soret M., van Staal C. and Bédard J.H., 2023. Geochemistry and geochronology of the Bay of Islands metamorphic sole, Newfoundland, Canada: Protoliths and implications for subduction initiation. GSA Bull., 136: 371-387. https://doi.org/10.1130/b36662.1

Gaggero L., Marroni M., Pandolfi L. and Buzzi L., 2009. Modeling the oceanic lithosphere obduction: constraints from the metamorphic sole of the Mirdita Ophiolites (Northern Albania). Ofioliti, 34: 17-42. https://doi.org/10.4454/ofioliti.v34i1.376

Gale A., Dalton C.A., Langmuir C.H., Su Y. and Schilling J.-G., 2013. The mean composition of ocean ridge basalts. Geochem. Geophys. Geosys., 14: 489-518. https://doi.org/10.1029/2012GC004334

Gamaleldien H., Li Z.-X., Abu Anbar M., Murphy J.B. and Doucet L.S., 2022. Geochronological and isotopic constraints on Neoproterozoic crustal growth in the Egyptian Nubian Shield: Review and synthesis. Earth-Science Rev., 235: 104244. https://doi.org/10.1016/j.earscirev.2022.104244

Garber J.M., Rioux M., Kylander-Clark A.R.C., Hacker B.R., Vervoort J.D. and Searle M.P., 2020. Petrochronology of Wadi Tayin Metamorphic Sole Metasediment, With Implications for the Thermal and Tectonic Evolution of the Samail Ophiolite (Oman/UAE). Tectonics, 39: e2020TC006135. https://doi.org/10.1029/2020TC006135

Garber J.M., Rioux M., Searle M.P., Kylander-Clark A.R.C., Hacker B.R., Vervoort J.D., Warren C.J. and Smye A.J., 2021. Dating Continental Subduction Beneath the Samail Ophiolite: Garnet, Zircon, and Rutile Petrochronology of the As Sifah Eclogites, NE Oman. J. Geophys. Res.: Solid Earth, 126: e2021JB022715. https://doi.org/10.1029/2021JB022715

Garber J.M., Rioux M., Smye A.J., Cruz-Uribe A.M., Baker P.L., Vervoort J.D., Searle M.P. and Feineman M.D., 2025. Shear heating during rapid subduction initiation beneath the Samail Ophiolite. Nature Geosci., 18: 653-660. https://doi.org/10.1038/s41561-025-01711-6

Ghent E.D. and Stout M.Z., 1981. Metamorphism at the Base of the Samail Ophiolite, Southeastern Oman Mountains. J. Geophys. Res., 86: 2557-2571. https://doi.org/10.1029/JB086iB04p02557

Glennie K.W., Boeuf M.G., Hughes-Clarke M.H.W., Moody-Stuart M., Pilaar W.G. and Reinhardt B.M., 1973. Late Cretaceous nappes in the Oman mountains and their geologic evolution. AAPG Bulletin, 57: 5-27. https://doi.org/10.1306/819A4240-16C5-11D7-8645000102C1865D

Gnos E., 1992. The metamorphic rocks associated with the Semail Ophiolite (Sultanate of Oman and United Arab Emirates). Bern University, Switzerland, 120 pp.

Gnos E., 1998. Peak Metamorphic Conditions of Garnet Amphibolites Beneath the Semail Ophiolite: Implications for an Inverted Pressure Gradient. Intern. Geol. Rev., 40: 281-304. https://doi.org/10.1080/00206819809465210

Godard M., Bosch D. and Einaudi F., 2006. A MORB source for low-Ti magmatism in the Semail ophiolite. Chem. Geol., 234: 58-78. https://doi.org/10.1016/j.chemgeo.2006.04.005

Godard M., Dautria J.M. and Perrin M., 2003. Geochemical variability of the Oman ophiolite lavas: Relationship with spatial distribution and paleomagnetic directions. Geochem. Geophys. Geosyst., 4: 8609. https://doi.org/10.1029/2002gc000452

Gómez-Pérez I., Morton A., Rawahi H.A. and Frei D., 2024. Oman as a fragment of Ediacaran eastern Gondwana. Geology, 52: 473-478. https://doi.org/10.1130/g51989.1

Goodenough K., Styles M., Schofield D., Thomas R., Crowley Q., Lilly R., McKervey J., Stephenson D. and Carney J., 2010. Architecture of the Oman–UAE ophiolite: Evidence for a multiphase magmatic history. Arab. J. Geosci., 3: 439-458. https://doi.org/10.1007/s12517-010-0177-3

Gray D.R., Gregory R.T., Armstrong R.A., Richards I.J. and Miller J.M., 2005. Age and Stratigraphic Relationships of Structurally Deepest Level Rocks, Oman Mountains: U/Pb SHRIMP Evidence for Late Carboniferous Neotethys Rifting. J. Geol., 113: 611-626. https://doi.org/10.1086/449325

Guilmette C., Hébert R., Wang C. and Villeneuve M., 2009. Geochemistry and geochronology of the metamorphic sole underlying the Xigaze Ophiolite, Yarlung Zangbo Suture Zone, South Tibet. Lithos, 112: 149-162. https://doi.org/10.1016/j.lithos.2009.05.027

Guilmette C., Smit M.A., van Hinsbergen D.J.J., Gürer D., Corfu F., Charette B., Maffione M., Rabeau O. and Savard D., 2018. Forced subduction initiation recorded in the sole and crust of the Semail Ophiolite of Oman. Nature Geosci., 11: 688-695. https://doi.org/10.1038/s41561-018-0209-2

Guilmette C., van Hinsbergen D.J.J., Smit M.A., Godet A., Fournier-Roy F., Butler J.P., Maffione M., Li S. and Hodges K., 2023. Formation of the Xigaze Metamorphic Sole under Tibetan continental lithosphere reveals generic characteristics of subduction initiation. Communications Earth & Environment, 4: 339. https://doi.org/10.1038/s43247-023-01007-w

Haase K.M., Freund S., Beier C., Koepke J., Erdmann M. and Hauff F., 2016. Constraints on the magmatic evolution of the oceanic crust from plagiogranite intrusions in the Oman ophiolite. Contrib. Mineral. Petrol., 171: 46. https://doi.org/10.1007/s00410-016-1261-9

Haase K.M., Freund S., Koepke J., Hauff F. and Erdmann M., 2015. Melts of sediments in the mantle wedge of the Oman ophiolite. Geology, 43: 275-278. https://doi.org/10.1130/G36451.1

Hacker B.R. and Gnos E., 1997. The conundrum of Samail: explaining the metamorphic history. Tectonophysics, 279: 215-226. http://dx.doi.org/10.1016/S0040-1951(97)00114-5

Hacker B.R. and Mosenfelder J.L., 1996. Metamorphism and deformation along the emplacement thrust of the Samail ophiolite, Oman. Earth Planet. Sci. Lett., 144: 435-451. https://doi.org/10.1016/S0012-821X(96)00186-0

Hacker B.R., Mosenfelder J.L. and Gnos E., 1996. Rapid emplacement of the Oman ophiolite: Thermal and geochronologic constraints. Tectonics, 15: 1230-1247. https://doi.org/10.1029/96tc01973

Hopson C.A., Coleman R.G., Gregory R.T., Pallister J.S. and Bailey E.H., 1981. Geologic section through the Samail ophiolite and associated rocks along a Muscat-Ibra transect, southeastern Oman Mountains. J. Geophys. Res., 86: 2527-2544. https://doi.org/10.1029/JB086iB04p02527

Ishikawa T., Fujisawa S., Nagaishi K. and Masuda T., 2005. Trace element characteristics of the fluid liberated from amphibolite-facies slab: Inference from the metamorphic sole beneath the Oman ophiolite and implication for boninite genesis. Earth Planet. Sci. Lett., 240: 355-377. http://dx.doi.org/10.1016/j.epsl.2005.09.049

Ishikawa T., Nagaishi K. and Umino S., 2002. Boninitic volcanism in the Oman ophiolite: Implications for thermal condition during transition from spreading ridge to arc. Geology, 30: 899-902. https://doi.org/10.1130/0091-7613(2002)030%3C0899:BVITOO%3E2.0.CO;2

Ishizuka O., Tani K., Reagan M.K., Kanayama K., Umino S., Harigane Y., Sakamoto I., Miyajima Y., Yuasa M. and Dunkley D.J., 2011. The timescales of subduction initiation and subsequent evolution of an oceanic island arc. Earth Planet. Sci. Lett., 306: 229-240. https://doi.org/10.1016/j.epsl.2011.04.006

Jackson S.E., Pearson N.J., Griffin W.L. and Belousova E.A., 2004. The application of laser ablation-inductively coupled plasma-mass spectrometry to in situ U–Pb zircon geochronology. Chem. Geol., 211: 47-69. https://doi.org/10.1016/j.chemgeo.2004.06.017

Jamieson R.A., 1986. P-T paths from high temperature shear zones beneath ophiolites. J. Metam. Geol., 4: 3-22. https://doi.org/10.1111/j.1525-1314.1986.tb00335.x

Janney P.E., Le Roex A.P. and Carlson R.W., 2005. Hafnium Isotope and Trace Element Constraints on the Nature of Mantle Heterogeneity beneath the Central Southwest Indian Ridge (13°E to 47°E). J. Petrol., 46: 2427-2464. https://doi.org/10.1093/petrology/egi060

Jansen M.N., MacLeod C.J., Lissenberg C.J., Parkinson I.J. and Condon D.J., 2024. Relationship Between D-MORB and E-MORB Magmatism During Crustal Accretion at Mid-Ocean Ridges: Evidence From the Masirah Ophiolite (Oman). Geochem. Geophys. Geosys., 25: e2023GC011361. https://doi.org/10.1029/2023GC011361

Jochum K.P., Weis U., Stoll B., Kuzmin D., Yang Q., Raczek I., Jacob D.E., Stracke A., Birbaum K., Frick D.A., Günther D. and Enzweiler J., 2011. Determination of Reference Values for NIST SRM 610–617 Glasses Following ISO Guidelines. Geost. Geoanal. Res., 35: 397-429. https://doi.org/10.1111/j.1751-908X.2011.00120.x

John T., Scherer E.E., Haase K. and Schenk v., 2004. Trace element fractionation during fluid-induced eclogitization in a subducting slab: trace element and Lu–Hf–Sm–Nd isotope systematics. Earth Planet. Sci. Lett., 227: 441-456. https://doi.org/10.1016/j.epsl.2004.09.009

Johnson T.A., Vervoort J.D., Ramsey M.J., Aleinikoff J.N. and Southworth S., 2018. Constraints on the timing and duration of orogenic events by combined Lu–Hf and Sm–Nd geochronology: An example from the Grenville orogeny. Earth Planet. Sci. Lett., 501: 152-164. https://doi.org/10.1016/j.epsl.2018.08.030

Keenan T.E., Encarnación J., Buchwaldt R., Fernandez D., Mattinson J., Rasoazanamparany C. and Luetkemeyer P.B., 2016. Rapid conversion of an oceanic spreading center to a subduction zone inferred from high-precision geochronology. Proc. Nat. Academ. Sci., 113: E7359-E7366. https://doi.org/10.1073/pnas.1609999113

Kim S., Jang Y., Kwon S., Samuel v.O., Kim S.W., Park S.-I., Santosh M. and Kokkalas S., 2020. Petro-tectonic evolution of metamorphic sole of the Semail ophiolite, UAE. Gondwana Res., 86: 203-221. https://doi.org/10.1016/j.gr.2020.05.013

Koepke J., Schoenborn S., Oelze M., Wittmann H., Feig S.T., Hellebrand E., Boudier F. and Schoenberg R., 2009. Petrogenesis of crustal wehrlites in the Oman ophiolite: Experiments and natural rocks. Geochem. Geophys. Geosyst., 10: Q10002. https://doi.org/10.1029/2009gc002488

Kotowski A.J., Cloos M., Stockli D.F. and Bos Orent E., 2021. Structural and Thermal Evolution of an Infant Subduction Shear Zone: Insights From Sub-Ophiolite Metamorphic Rocks Recovered From Oman Drilling Project Site BT-1B. J. Geophys. Res.: Solid Earth, 126: e2021JB021702. https://doi.org/10.1029/2021JB021702

Kusano Y., Adachi Y., Miyashita S. and Umino S., 2012. Lava accretion system around mid-ocean ridges: Volcanic stratigraphy in the Wadi Fizh area, northern Oman ophiolite. Geochem. Geophys. Geosyst., 13: Q05012. https://doi.org/10.1029/2011gc004006

Kylander-Clark A.R.C., Hacker B.R. and Cottle J.M., 2013. Laser-ablation split-stream ICP petrochronology. Chem. Geol., 345: 99-112. http://dx.doi.org/10.1016/j.chemgeo.2013.02.019

Lippard S.J. and Rex D.C., 1982. K—Ar ages of alkaline igneous rocks in the northern Oman mountains, NE Arabia, and their relations to rifting, passive margin development and destruction of the Oman Tethys. Geol. Mag., 119: 497-503. https://doi.org/10.1017/S0016756800026844

Lippard S.J., Shelton A.W. and Gass I.G., 1986. The Ophiolite of Northern Oman. Geol. Soc. London, London, 178 pp.

Mackay-Champion T.C., Searle M.P., Tapster S., Roberts N.M.W., Shail R.K., Palin R.M., Willment G.H. and Evans J.T., 2024. Magmatic, Metamorphic and Structural History of the Variscan Lizard Ophiolite and Metamorphic Sole, Cornwall, UK. Tectonics, 43: e2023TC008187. https://doi.org/10.1029/2023TC008187

MacLeod C.J., Lissenberg C.J. and Bibby L.E., 2013. “Moist MORB” axial magmatism in the Oman ophiolite: The evidence against a mid-ocean ridge origin. Geology, 41: 459-462. https://doi.org/10.1130/G33904.1

Malpas J., 1979. The dynamothermal aureole of the Bay of Islands ophiolite suite. Can. J. Earth Sci., 16: 2086-2101. https://doi.org/10.1139/e79-198

Marie B., Marin L., Martin P.-Y., Gulon T., Carignan J. and Cloquet C., 2015. Determination of Mercury in One Hundred and Sixteen Geological and Environmental Reference Materials Using a Direct Mercury Analyser. Geost. Geoanal. Res., 39: 71-86. https://doi.org/10.1111/j.1751-908X.2013.00254.x

McDonough W.F. and Sun S.s., 1995. The composition of the Earth. Chem. Geol., 120: 223-253. http://dx.doi.org/10.1016/0009-2541(94)00140-4

Meinhold G., Bassis A., Hinderer M., Lewin A. and Berndt J., 2021. Detrital zircon provenance of north Gondwana Palaeozoic sandstones from Saudi Arabia. Geol. Mag., 158: 442-458. https://doi.org/10.1017/S0016756820000576

Mertzman S., 2000. K-Ar results from the southern Oregon-northern California Cascade Range. Oregon Geology, 62: 99-122.

Miyashiro A., 1973. The Troodos ophiolitic complex was probably formed in an island arc. Earth Planet. Sci. Lett., 19: 218-224. https://doi.org/10.1016/0012-821X(73)90118-0

Nicolas A., Boudier F., Ildefonse B. and Ball E., 2000. Accretion of Oman and United Arab Emirates ophiolite – Discussion of a new structural map. Mar. Geophys. Res., 21: 147-180. https://doi.org/10.1023/a:1026769727917

Niu Y., Collerson K.D., Batiza R., Wendt J.I. and Regelous M., 1999. Origin of enriched-type mid-ocean ridge basalt at ridges far from mantle plumes: The East Pacific Rise at 11°20’N. J. Geophys. Res.: Solid Earth, 104: 7067-7087. https://doi.org/10.1029/1998JB900037

O’Neill H.S.C., 2016. The Smoothness and Shapes of Chondrite-normalized Rare Earth Element Patterns in Basalts. J. Petrol., 57: 1463-1508. https://doi.org/10.1093/petrology/egw047

Pallister J.S. and Hopson C.A., 1981. Samail ophiolite plutonic suite: Field relations, phase variation, cryptic variation and layering, and a model of a spreading ridge magma chamber. J. Geophys. Res., 86: 2593-2644. https://doi.org/10.1029/JB086iB04p02593

Parkinson C., 1998. Emplacement of the East Sulawesi Ophiolite: evidence from subophiolite metamorphic rocks. J. Asian Earth Sci., 16: 13-28. https://doi.org/10.1016/S0743-9547(97)00039-1

Paton C., Hellstrom J., Paul B., Woodhead J. and Hergt J., 2011. Iolite: Freeware for the visualisation and processing of mass spectrometric data. J. Anal. Atom. Spectrom., 26: 2508-2518. https://doi.org/10.1039/C1JA10172B

Pearce J.A., 1983. Role of the Sub-Continental Lithosphere in Magma Genesis at Active Continental Margins, In: Hawkesworth, C.J., Norry, M.J. (Eds.). Continental Basalts and Mantle Xenoliths, Shiva Publishing, Cheshire, UK; 230-249.

Pearce J.A., 1996. A User’s Guide to Basalt Discrimination Diagrams. Trace Element Geochemistry of Volcanic Rocks: Applications for Massive Sulphide Exploration: Geological Association of Canada, Short Course Notes, 12: 79-113.

Pearce J.A., 2008. Geochemical fingerprinting of oceanic basalts with applications to ophiolite classification and the search for Archean oceanic crust. Lithos, 100: 14-48. https://doi.org/10.1016/j.lithos.2007.06.016

Pearce J.A., Alabaster T., Shelton A.W. and Searle M.P., 1981. The Oman ophiolite as a Cretaceous arc-basin complex: Evidence and implications. Phil. Trans. Roy. Soc. London. Series A, Mathematical and Physical Sciences, 300: 299-317. https://doi.org/10.1098/rsta.1981.0066

Pearce J.A., Lippard S.J. and Roberts S., 1984. Characteristics and tectonic significance of supra-subduction zone ophiolites. Geol. Soc.London, Spec. Publ., 16: 77-94. https://doi.org/10.1144/GSL.SP.1984.016.01.06

Penniston-Dorland S.C., Kohn M.J. and Manning C.E., 2015. The global range of subduction zone thermal structures from exhumed blueschists and eclogites: Rocks are hotter than models. Earth Planet. Sci. Lett., 428: 243-254. http://dx.doi.org/10.1016/j.epsl.2015.07.031

Perfit M.R., Fornari D.J., Smith M.C., Bender J.F., Langmuir C.H. and Haymon R.M., 1994. Small-scale spatial and temporal variations in mid-ocean ridge crest magmatic processes. Geology, 22: 375-379. 10.1130/0091-7613(1994)022<0375:Sssatv>2.3.Co;2

Prigent C., Guillot S., Agard P., Lemarchand D., Soret M. and Ulrich M., 2018. Transfer of subduction fluids into the deforming mantle wedge during nascent subduction: Evidence from trace elements and boron isotopes (Semail ophiolite, Oman). Earth Planet. Sci. Lett., 484: 213-228. https://doi.org/10.1016/j.epsl.2017.12.008

Prinzhofer A., Lewin E. and Allègre C.J., 1989. Stochastic melting of the marble cake mantle: evidence from local study of the East Pacific Rise at 12°50'N. Earth Planet. Sci. Lett., 92: 189-206. https://doi.org/10.1016/0012-821X(89)90046-0

Reichen L. and Fahey J., 1962. An improved method for the determination of FeO in rocks and minerals including garnet, Geol. Surv. Bulletin 1144B.

Ring U., Glodny J., Hansman R., Scharf A., Mattern F., Callegari I., van Hinsbergen D.J.J., Willner A. and Hong y., 2024. The Samail subduction zone dilemma: Geochronology of high-pressure rocks from the Saih Hatat window, Oman, reveals juxtaposition of two subduction zones with contrasting thermal histories. Earth-Science Rev., 250: 104711. https://doi.org/10.1016/j.earscirev.2024.104711

Rioux M., Benoit M., Amri I., Ceuleneer G., Garber J.M., Searle M. and Leal K., 2021a. The Origin of Felsic Intrusions Within the Mantle Section of the Samail Ophiolite: Geochemical Evidence for Three Distinct Mixing and Fractionation Trends. J. Geophys. Res. Solid Earth, 126: e2020JB020760. https://doi.org/10.1029/2020JB020760

Rioux M., Bowring S., Kelemen P., Gordon S., Miller R. and Dudás F., 2013. Tectonic development of the Samail ophiolite: High-precision U-Pb zircon geochronology and Sm-Nd isotopic constraints on crustal growth and emplacement. J. Geophys. Res. Solid Earth, 118: 2085-2101. https://doi.org/10.1002/jgrb.50139

Rioux M., Bowring S.A., Kelemen P.B., Gordon S., Dudás F. and Miller R., 2012. Rapid crustal accretion and magma assimilation in the Oman-U.A.E. ophiolite: High precision U-Pb zircon geochronology of the gabbroic crust. J. Geophys. Res., 117. https://doi.org/10.1029/2012JB009273

Rioux M., Garber J., Bauer A., Bowring S., Searle M., Kelemen P. and Hacker B., 2016. Synchronous formation of the metamorphic sole and igneous crust of the Semail ophiolite: New constraints on the tectonic evolution during ophiolite formation from high-precision U–Pb zircon geochronology. Earth Planet. Sci. Lett., 451: 185-195. http://dx.doi.org/10.1016/j.epsl.2016.06.051

Rioux M., Garber J.M., Searle M., Crowley J.L., Stevens S., Schmitz M., Kylander-Clark A., Leal K., Ambrose T. and Smye A.J., 2023. The temporal evolution of subduction initiation in the Samail ophiolite: High-precision U-Pb zircon petrochronology of the metamorphic sole. J. Metam. Geol., 41: 817-847. https://doi.org/10.1111/jmg.12719

Rioux M., Garber J.M., Searle M., Kelemen P., Miyashita S., Adachi Y. and Bowring S., 2021b. High-Precision U-Pb Zircon Dating of Late Magmatism in the Samail Ophiolite: A Record of Subduction Initiation. J. Geophys. Res. Solid Earth, 126: e2020JB020758. https://doi.org/10.1029/2020JB020758

Roberts N.M.W., Thomas R.J. and Jacobs J., 2016. Geochronological constraints on the metamorphic sole of the Semail ophiolite in the United Arab Emirates. Geosci. Front., 7: 609-619. https://doi.org/10.1016/j.gsf.2015.12.003

Robinson F.A., Foden J.D., Collins A.S. and Payne J.L., 2014. Arabian Shield magmatic cycles and their relationship with Gondwana assembly: Insights from zircon U–Pb and Hf isotopes. Earth Planet. Sci. Lett., 408: 207-225. https://doi.org/10.1016/j.epsl.2014.10.010

Rollinson H., 2015. Slab and sediment melting during subduction initiation: granitoid dykes from the mantle section of the Oman ophiolite. Contrib. Mineral. Petrol., 170: 1-20. https://doi.org/10.1007/s00410-015-1177-9

Roy N.K. and Bose S.S., 2008. Determination of Mercury in Thirty-three International Stream Sediment and Soil Reference Samples by Direct Mercury Analyser. Geostandards and Geoanalytical Research, 32: 331-335. https://doi.org/10.1111/j.1751-908X.2008.00851.x

Savci G., 1988. Structural and metamorphic geology of the subophiolitic dynamothermal metamorphic sole and peridotite tectonites, Blow Me Down massif, Newfoundland-Canada: Tectonic implications for subduction and obduction. University of Houston, United States, 379 pp.

Searle M., Rioux M. and Garber J.M., 2022. One line on the map: A review of the geological history of the Semail Thrust, Oman-UAE mountains. J. Struct. Geol., 158: 104594. https://doi.org/10.1016/j.jsg.2022.104594

Searle M.P., 1984. Alkaline peridotite, pyroxenite, and gabbroic intrusions in the Oman Mountains, Arabia. Can. J. Earth Sci., 21: 396-406. https://doi.org/10.1139/e84-043

Searle M.P., 2007. Structural geometry, style and timing of deformation in the Hawasina Window, Al Jabal al Akhdar and Saih Hatat culminations, Oman Mountains. GeoArabia, 12: 99-130. https://doi.org/10.2113/geoarabia120299

Searle M.P. and Cox J., 2002. Subduction zone metamorphism during formation and emplacement of the Semail ophiolite in the Oman Mountains. Geol. Mag., 139: 241-255. https://doi.org/10.1017/S0016756802006532

Searle M.P., Garber J.M. and Rioux M., 2025. Structure of the NE Oman Mountains: A Review of Robust Geochronological Constraints for Tectonic Models of Ophiolite Obduction and Continental Subduction. Tectonics, 44: e2025TC008834. https://doi.org/10.1029/2025TC008834

Searle M.P. and Graham G.M., 1982. "Oman Exotics"—Oceanic carbonate build-ups associated with the early stages of continental rifting. Geology, 10: 43-49. https://doi.org/10.1130/0091-7613(1982)10<43:Oecbaw>2.0.Co;2

Searle M.P., Lippard S.J., Smewing J.D. and Rex D.C., 1980. Volcanic rocks beneath the Semail Ophiolite nappe in the northern Oman mountains and their significance in the Mesozoic evolution of Tethys. J. Geol. Soc., London, 137: 589-604. https://doi.org/10.1144/gsjgs.137.5.0589

Searle M.P. and Malpas J., 1980. The structure and metamorphism of rocks beneath the Semail Ophiolite of Oman and their significance in ophiolite obduction. Trans. Roy. Soc. Edinburgh, Earth Sci., 71: 247–262. https://doi.org/10.1017/S0263593300013614

Searle M.P. and Malpas J., 1982. Petrochemistry and origin of sub-ophiolitic metamorphic and related rocks in the Oman Mountains. J. Geol. Soc., London, 139: 235-248. https://doi.org/10.1144/gsjgs.139.3.0235

Šegvić B., Slovenec D., Altherr R., Babajić E., Mählmann R.F. and Lugović B., 2018. Petrogenesis of high-grade metamorphic soles from the Central Dinaric Ophiolite belt and their significance for the Neotethyan evolution in the Dinarides. Ofioliti, 44: 1-30. https://doi.org/10.4454/ofioliti.v44i1.514

Seton M., Müller R.D., Zahirovic S., Gaina C., Torsvik T., Shephard G., Talsma A., Gurnis M., Turner M., Maus S and Chandler M., 2012. Global continental and ocean basin reconstructions since 200Ma. Earth-Science Rev., 113: 212-270. https://doi.org/10.1016/j.earscirev.2012.03.002

Shen J., Dai J.-G., Yang K. and Zhang L.-L., 2025. Protracted subduction initiation of the Neo-Tethys: Insights from metamorphic sole chronology. Geology, 53: 803-808. 10.1130/g53409.1

Shervais J.W., 1982. Ti-V plots and the petrogenesis of modern and ophiolitic lavas. Earth Planet. Sci. Lett., 59: 101-118. https://doi.org/10.1016/0012-821x(82)90120-0

Sláma J., Košler J., Condon D.J., Crowley J.L., Gerdes A., Hanchar J.M., Horstwood M.S.A., Morris G.A., Nasdala L., Norberg N., Schaltegger U., Schoene B., Tubrett M.N. and Whitehouse M.J., 2008. Plešovice zircon - A new natural reference material for U-Pb and Hf isotopic microanalysis. Chem. Geol., 249: 1-35. https://doi.org/10.1016/j.chemgeo.2007.11.005

Soret M., Agard P., Dubacq B., Plunder A. and Yamato P., 2017. Petrological evidence for stepwise accretion of metamorphic soles during subduction infancy (Semail ophiolite, Oman and UAE). J. Metam. Geol., 35: 1051-1080. https://doi.org/10.1111/jmg.12267

Soret M., Agard P., Ildefonse B., Dubacq B., Prigent C. and Rosenberg C., 2019. Deformation mechanisms in mafic amphibolites and granulites: record from the Semail metamorphic sole during subduction infancy. Solid Earth, 10: 1733-1755. https://doi.org/10.5194/se-10-1733-2019

Soret M., Bonnet G., Agard P., Larson K.P., Cottle J.M., Dubacq B., Kylander-Clark A.R.C., Button M. and Rividi N., 2022. Timescales of subduction initiation and evolution of subduction thermal regimes. Earth Planet. Sci. Lett., 584: 117521. https://doi.org/10.1016/j.epsl.2022.117521

Spencer C.J., Cavosie A.J., Raub T.D., Rollinson H., Jeon H., Searle M.P., Miller J.A., McDonald B.J., Evans N.J. and Facility t.E.I.M., 2017. Evidence for melting mud in Earth's mantle from extreme oxygen isotope signatures in zircon. Geology, 45: 975-978. https://doi.org/10.1130/g39402.1

Stern B., Ali K., Liégeois J.P., Johnson P., Wiescek W. and Kattan F., 2010. Distribution and Significance of pre-Neoproterozoic Zircons in Juvenile Neoproterozoic Igneous Rocks of the Arabian-Nubian Shield. Amer. J. Sci., 310: 791. https://doi.org/10.2475/09.2010.02

Stern R.J. and Johnson P., 2010. Continental lithosphere of the Arabian Plate: A geologic, petrologic, and geophysical synthesis. Earth-Science Rev., 101: 29-67. https://doi.org/10.1016/j.earscirev.2010.01.002

Syracuse E.M., van Keken P.E. and Abers G.A., 2010. The global range of subduction zone thermal models. Phys. Earth Planet. Int., 183: 73-90. http://dx.doi.org/10.1016/j.pepi.2010.02.004

Tilton G.R., Hopson C.A. and Wright J.E., 1981. Uranium-lead isotopic ages of the Samail ophiolite, Oman, with applications to Tethyan ocean ridge tectonics. J. Geophys. Res., 86: 2763–2775. https://doi.org/10.1029/JB086iB04p02763

Ullah I., Xue C., Kakar M.I., Xie Z., Wang W., Ghaffar A. and Ullah N., 2021. Petrological and geochemical characterization of metamorphic sole rocks beneath the RasKoh ophiolite, western Pakistan: Implication for a Late Cretaceous supra-subduction zone-type forearc. Geol. J., 56: 5673-5690. https://doi.org/10.1002/gj.4264

Valera G.T.V., Kawakami T. and Payot B.D., 2022a. Mixing, fluid infiltration, leaching, and deformation (MILD) processes on the slab-mantle wedge interface at high T and P conditions: Records from the Dalrymple Amphibolite, Philippines. Chem. Geol., 604: 120941. https://doi.org/10.1016/j.chemgeo.2022.120941

Valera G.T.V., Kawakami T. and Payot B.D., 2022b. The slab–mantle wedge interface of an incipient subduction zone: Insights from the P–T–D evolution and petrological characteristics of the Dalrymple Amphibolite, Palawan Ophiolite, Philippines. J. Metam. Geol., 40: 717-749. https://doi.org/10.1111/jmg.12644

Valera G.T.V., Payot B.D., Kawakami T., Sakata S., Niki S. and Hirata T., 2026. From spreading to subduction: Timelines of induced subduction zones recorded in the Central Palawan Ophiolite. Lithos, 522-523: 108346. https://doi.org/10.1016/j.lithos.2025.108346

Vermeesch P., 2018. IsoplotR: A free and open toolbox for geochronology. Geosci. Front., 9: 1479-1493. https://doi.org/10.1016/j.gsf.2018.04.001

Wakabayashi J. and Dilek Y., 2000. Spatial and temporal relationships between ophiolites and their metamorphic soles: A test of models of forearc ophiolite genesis. Geol. Soc. Amer. Spec. Papers, 349: 53-64. https://doi.org/10.1130/0-8137-2349-3.53

Wakabayashi J. and Dilek Y., 2003. What constitutes 'emplacement' of an ophiolite?: Mechanisms and relationship to subduction initiation and formation of metamorphic soles. Geol. Soc., London, Spec. Publ., 218: 427-447. https://doi.org/10.1144/gsl.sp.2003.218.01.22

Warren C., Parrish R., Waters D. and Searle M., 2005. Dating the geologic history of Oman's Semail ophiolite: Insights from U-Pb geochronology. Contrib. Mineral. Petrol., 150: 403-422. https://doi.org/10.1007/s00410-005-0028-5

Waters C.L., Sims K.W.W., Perfit M.R., Blichert-Toft J. and Blusztajn J., 2011. Perspective on the Genesis of E-MORB from Chemical and Isotopic Heterogeneity at 9–10°N East Pacific Rise. J. Petrol., 52: 565-602. https://doi.org/10.1093/petrology/egq091

Waterton P., Pearson D.G., Mertzman S.A., Mertzman K.R. and Kjarsgaard B.A., 2020. A Fractional Crystallization Link between Komatiites, Basalts, and Dunites of the Palaeoproterozoic Winnipegosis Komatiite Belt, Manitoba, Canada. J. Petrol., 61. https://doi.org/10.1093/petrology/egaa052

Wiedenbeck M., Allé P., Corfu F., Griffin W.L., Meier M., Oberli F., Quadt A.V., Roddick J.C. and Spiegel W., 1995. Three natural zircon standards for U-Th-Pb, Lu-Hf, trace element and REE analyses. Geost. Newslett., 19: 1-23. https://doi.org/10.1111/j.1751-908X.1995.tb00147.x

Williams H. and Smyth W.R., 1973. Metamorphic aureoles beneath ophiolite suites and alpine peridotites; tectonic implications with west Newfoundland examples. Amer. J. Sci., 273: 594-621.

Winchester J.A. and Floyd P.A., 1977. Geochemical discrimination of different magma series and their differentiation products using immobile elements. Chem. Geol., 20: 325-343. https://doi.org/10.1016/0009-2541(77)90057-2

Xin G.-Y., Chu Y., Su B.-X., Lin W., Uysal I. and Feng Z.-T., 2021. Rapid transition from MORB-type to SSZ-type oceanic crust generation following subduction initiation: insights from the mafic dikes and metamorphic soles in the Pozantı-Karsantı ophiolite, SE Turkey. Contrib. Mineral. Petrol., 176: 64. https://doi.org/10.1007/s00410-021-01821-5

Yakymchuk C., Kirkland C.L. and Clark C., 2018. Th/U ratios in metamorphic zircon. J. Metam. Geol., 36: 715-737. https://doi.org/10.1111/jmg.12307

Yang S., Humayun M. and Salters v.J.M., 2020. Elemental constraints on the amount of recycled crust in the generation of mid-oceanic ridge basalts (MORBs). Sci. Adv., 6: eaba2923. https://doi.org/10.1126/sciadv.aba2923

Yoshikawa M., Python M., Tamura A., Arai S., Takazawa E., Shibata T., Ueda A. and Sato T., 2015. Melt extraction and metasomatism recorded in basal peridotites above the metamorphic sole of the northern Fizh massif, Oman ophiolite. Tectonophysics, 650: 53-64. https://doi.org/10.1016/j.tecto.2014.12.004

Ziegler U., Stössel F. and Peters T., 1991a. Meta-Carbonatites in the Metamorphic Series Below the Semail Ophiolite in the Dibba Zone, Northern Oman Mountains. Springer Netherlands, Dordrecht, pp. 627-645.

Ziegler U.R.F., Stoessel G.F.U. and Peters T., 1991b. Isotopic (Rb-Sr and Sm-Nd) and geochemical studies of the metamorphosed volcanic rocks in the metamorphic series below the Semail ophiolite in the Dibba zone (United Arab Emirates). Schweiz. Mineral. Petrogr. Mitt., 71: 19-33.

Received, April 1, 2026
Accepted, July 2, 2026